POLITECNICO DI MILANO
Facoltà di Ingegneria Industriale e dell' Informazione
Corso di Laurea Magistrale in Ingegneria Aeronautica

Development of a wind farm controller and wind farm control algorithm for wind tunnel testing

Relatore: Prof. Carlo Luigi Bottasso
Correlatore: Ing. Filippo Campagnolo

Tesi di Laurea di:
Nicola Troiano, matricola 782786

Anno Accademico 2012-2013

A mio padre, che ogni giorno si spacca
la schiena per amore dei suoi figli.
A mia madre, che ogni giorno con grande
amore mi fa sempre trovare un piatto caldo e una
casa pulita ed ordinata in cui potermi riposare.

Ringraziamenti

In primo luogo, vorrei ringraziare il prof. Carlo Bottasso per avermi dato la possibilità di intraprendere un lavoro di tesi così interessante e avermi fornito tutti gli strumenti necessari per portarlo a termine.

Un grande ringraziamento va all'ing. Filippo Campagnolo, che con grande dedizione mi ha seguito e accompagnato in questi mesi di lavoro, sopportando le mie numerosissime sviste e distrazioni con grande pazienza e insegnandomi ad usare un po' più la testa e a ragionare da ingegnere.

Vorrei ringraziare anche Federico Carlo e Stefano per il grande supporto morale (e spesso anche pratico) che mi hanno dato, in particolar modo negli ultimi 3 mesi, spesso anche solo con un gesto di cortesia o con un saluto.

> *...quando vedo crollare quello in cui credo, poi mi sollevo e riparto da zero e so che ogni cosa la devo alle palle quadre di mio padre e al suo sudore, al sorriso di mia madre, al viso di ogni nonno che proietta amore, a mio fratello piccolo ora più alto di me, nonna mi protegge sulla stella più bella che c'è...*

Con le semplici parole di una canzone degli Articolo 31, il mio primo ringraziamento va ai miei genitori, per avermi sempre sostenuto, per aver creduto nelle mie capacità sin dall'infanzia, per avermi sempre insegnato a dare sempre il meglio di me e a mettere a frutto le capacità e i doni che ho ricevuto. Un grazie va anche a mio fratello, perchè nonostante i mille litigi e incomprensioni ha sempre dimostrato di stimarmi e di volermi bene dal profondo del cuore.

Un grazie gratuito, nonchè doveroso, va ad Elisa, la cui esplosività, caparbietà, testardaggine, intelligenza, curiosità, tenerezza e soprattutto Amore hanno accompagnato, accompagnano e, a questo punto, continueranno ad accompagnare ogni singolo momento della mia vita, rendendomi ogni giorno sempre più un uomo. La tua presenza ed il tuo amore sono stati "luce e sale", perchè hanno illuminato ogni momento di buio di questo lungo cammino in

cui avrei rischiato di perdermi e sale perchè hanno dato il senso e il sapore a questa esperienza.

Un grazie va a tutti i miei amici, in particolar modo Emanuele, Marco, Simone, Marco, Gabriele, Debora, Chiara Francesca e Guido, per aver sempre condiviso le gioie e le difficoltà in modo sincero e gratuito, spesso accompagnandole con una bella birra.

Un ringraziamento va anche a Francesca, Michele, Andrea, Sara, Marco e Chiara, per aver sempre dimostrato un amicizia salda e radicata in Cristo, soprattutto nei momenti più difficili.

Un grazie a Zaga, Miki e Teo, che in questi cinque anni hanno condiviso questo calvario, la cui compagnia è stata di fondamentale importanza e mi ha permesso di preservare un po' della mia sanità mentale, ammesso e non concesso che prima ce ne fosse.

Un grazie lo dedico al maestro Alessandro Tulis, a Michele, Luca, Ivano, Andrea, Andrea, Luca e a tutti gli allievi del Karate-do Rei, perchè sul tatami, fra sangue e sudore ho imparato che nella vita l'importante è non mollare mai e continuare a combattere. OSS!

Ringrazio anche a tutte quelle persone che nei modi più disparati e fantasiosi hanno cercato di gettare le tenebre nella mia vita, facendomi arrancare e vacillare, perchè grazie a voi ho trovato nuove forze e nuovo coraggio di affrontare la vita. Un grazie a tutti quelli che non hanno mai creduto in me e che null' altro hanno cercato che distruggere la mia autostima, perchè nonostante tutto questo, io ce l'ho fatta!!!

A chi molto è stato dato, molto sarà richiesto;
e a chi molto è stato affidato, tanto più si richiederà
Lc 12,48

Contents

List of Figures

List of Tables

Sommario

Negli ultimi anni, la produzione di energia attraverso fonti rinnovabili, in particolar modo l'energia eolica, stanno vivendo un momento di grande espansione. Questo incremento ha reso necessaria l'organizzazione di queste macchine in grandi parchi eolici al fine di limitare gli spazi occupati.

L'organizzazione delle macchine in parchi eolici porta, tuttavia, a fenomeni di interazione della scia generata dalle macchine poste a monte su quelle poste a valle del vento, che si traducono in un calo delle prestazioni delle ultime e quindi ad una riduzione delle prestazioni dell'intero parco eolico.

Di fronte a questo problema, la ricerca sta dedicando numerose energie al fine di migliorare le prestazioni complessive dei parchi eolici, sviluppando numerosi approcci, primo fra tutti quello numerico.

In questo lavoro è stato affrontato lo sviluppo di un controllore real-time di un parco eolico composto da due macchine per la sperimentazione di leggi di controllo in galleria del vento.

Nella prima parte, viene spiegata la politica di controllo, chiamata parzializzazione ISO-TSR, che è stata sviluppata al fine di ridurre la potenza generata dalla macchina posta a monte, riducendo così gli effetti della propria scia su quella posta a valle. La politica di controllo si basa sull'invio di un set-point di potenza, richiedendo a ciascuna macchina l'erogazione di una certa percentuale della potenza disponibile date le condizione di vento.

Nella seconda parte, viene descritto in modo dettagliato il funzionamento e lo sviluppo del controllore e la logica di funzionamento della modalità manuale ed automatica. Nella modalità automatica, il controllore ricerca la parzializzazione che ottimizza la potenza prodotta attraverso l' algoritmo "Simulated Annealing".

Infine, vengono mostrati i risultati ottenuti dai test effettuati al banco prova. Viene mostrata la capacità di inseguire le traiettorie parzializzate con il metodo ISO-TSR in ogni condizione di vento, la capacità di passare da una parzializzazione ad un'altra e la capacità del controllore di realizzare un controllo real-time in galleria del vento.

Parole chiave:Parchi eolici, controllo, galleri del vento, simulated annealing, approccio ISO-TSR.

Abstract

In the last years, the energy production based on renewable energies and particularly wind energy, is experiencing a period of great expansion. This increase has lead to the need to organize the wind turbines in wind farms in order to reduce the occupied areas.

However, the compression of the wind turbines in wind farm has lead to interaction phenomenon of the wakes generated by the upstream wind turbines on the downstream ones, that generate a drop in the wind farm total power production.

In this overview, the research is focusing the attention on this problem, in order to improve the wind farm performance, developing different approaches, first among everything the numerical one.

In the present work a real-time controller able to control a wind farm made up of two wind turbines for wind tunnel application has been developed.

In the first part, the author explain how the ISO-TSR partialization works, i.e. the control policy that has been developed in order to reduce the power of upstream wind turbine and so the effects of the its wake on the downstream one. The control policy consists in a power set-point sending, asking to the wind turbine a certain percentage of the power available in that wind condition.

In the second part, the author explain how the wind farm controller works, its development and the functioning logic of the automatic and manual modes. In the automatic mode, the controller try to optimize the power production of the complete wind farm through a "Simulated Annealing" algorithm.

As a conclusion, the results obtained through the test bench testing are presented. The ability of controller to follow a trajectory partialized with the ISO-TSR approach, as well as the ability to switch from a partilization to another is demonstrated. Eventually, the ability of the controller to realize a real-time control in the wind tunnel is shown.

Keywords:Wind farm, control, wind tunnel, simulated annealing, ISO-TSR approach.

Riassunto

Il crescente costo di tutti i prodotti ricavati dai combustibili fossili, unitamente alla cresciuta sensibilità da parte della società moderna volta alla riduzione delle emissioni inquinanti, sta portando molto rapidamente allo sviluppo di fonti di energia rinnovabili. In questo contesto l'energia eolica sta ricomprendo un ruolo fondamentale e negli ultimi anni ha vissuto un periodo di grande sviluppo che secondo le previsioni è destinato a proseguire positivamente.

L'aumento del numero di generatori eolici tuttavia ha portato necessariamente ad una loro organizzazione in contesti di wind farm, che consentono una compattazione e una riduzione degli spazi occupati dalle macchine.

L'organizzazione di queste macchine in contesti di wind farm porta, tuttavia a fenomeni di interazione fra le stesse, in particolar modo, la scia delle macchine poste a monte si riflette negativamente sulle macchine poste a valle del vento, riducendo di molto la potenza prodotta dalle ultime e quindi complessivamente la potenza prodotta da tutta la wind farm.

Solo negli ultimi anni, la ricerca ha iniziato ad investire energie nello sviluppo di tecniche che consentano di ottimizzare la potenza prodotta, nella prospettiva di ridurre il costo dell'energia, rendendo l'energia eolica ancor più competitiva dal punto di vista economico.

Dal momento questo ambito della ricerca in campo eolico risulta essere molto giovane, si stanno sviluppando molto velocemente numerose tecniche: la disposizione ottima delle macchine all'interno della wind farm, lo sviluppo di modelli matematici di scia sempre più complessi, che siano in grado di rendere le simulazioni numeriche sempre più affidabili, i test su grande scala e non da ultimo la ricerca in galleria del vento.

Le simulazioni numeriche rappresentano l'approccio più comune a questi problemi, dal momento che consentono di studiare i fenomeni fisici con l'ausilio di computer. Tuttavia, presentano un forte limite, ovvero la simulazione numerica di wind farm prevede lo studio dell'interazione della scia, che è caratterizzata da una forte turbolenza, con le macchine poste a valle. L'analisi di questo tipo di fenomeni fisici, tuttavia, per quanto possa essere accompagnato da una forte potenza di calcolo, richiede numerose ore, senza considerare

il fatto che i modelli matematici che caratterizzano i fenomeni di turbolenza non sono completamente attendibili.

La ricerca in galleria del vento, da un lato, rappresenta un limite, perchè sono necessarie delle strutture adatte ad ospitare queste macchine e perchè è altresì necessario studiare in maniera opportuna le leggi di scalatura della macchine, in maniera tale da poter riprodurre in modo fedele il comportamento della macchina sia dal punto di vista aerodinamico, sia dal punto di vista dell'elasticità della struttura. Da un altro lato, invece, rappresenta uno strumento di grande rilevanza, soprattutto nello studio di leggi di controllo che riguardano l'interazione fra le macchine e la scia. Infatti, basti pensare che all'interno della galleria del vento le macchine poste a valle possono essere investite da una scia reale e non simulata o ricreata numericamente sulla base di un modello matematico. La galleria del vento consente inoltre di lavorare in un contesto sicuro e controllato e di ridurre notevolmente il tempo necessario alla simulazione.

Il progetto argomento di questo tesi è stato lo sviluppo di un controllore real-time di wind farm in grado di ottimizzare la potenza prodotta da una wind farm composta di due macchine per la sperimentazione in galleria del vento.

Nel Capitolo 2, viene presentata la strumentazione che si è resa necessaria durante il progetto, spiegando in maniera piuttosto dettagliata i modelli V2 sviluppati dal Politecnico di Milano nell'ambito di un progetto pluriennale con la società Vestas.

L'obbiettivo di questa collaborazione è stata la realizzazione di un modello in scala ridotta della Vestas V90 per la sperimentazione in galleria del vento di leggi di controllo. A seguito di questo progetto è stato realizzato un secondo modello, identico al primo, aprendo così la strada alle prime sperimentazioni in galleria del vento di leggi di controllo per le wind farm.

I modelli vengono descritti nei loro particolari, descrivendo i sensori installati sulla macchina, gli attuatori, la logica di funzionamento del sistema di controllo e gli strumenti utilizzati per la calibrazione del controllore.

Nel Capitolo 3, viene invece descritto in modo dettagliato il modo in cui è stato sviluppato il controllore e la sua logica di funzionamento. Il capitolo inizia presentando la logica di controllo tradizionale della macchina isolata, descrivendo come vengono calcolate le traiettorie di regolazione in Regione II, II$^1/_2$ e III e la modalità con cui viene realizzato il controllo in coppia e in passo pala.

Successivamente, il capitolo prosegue nella descrizione del modo in cui la logica di controllo è stata modificata, al fine di poter richiedere alla macchina l'erogazione solo di una percentuale della potenza disponibile, riducendo così l'intensità della scia e quindi consentendo alla macchina posta a monte del

vento di ricevere un beneficio in termini di potenza. Il metodo sviluppato è stata rinominato "parzializzazione ISO-TSR". Il metodo viene sviluppato a partire dall'equazione della potenza della macchina:

$$P = \frac{1}{2}\rho A V^3 C_P$$

Dall'equazione si può facilmente notare che l'unico termine su cui il controllo della macchina può intervenire è il termine C_P, ad esempio, moltiplicandolo per un coefficiente $p \in [0, 1]$. Analizzando i grafici $C_P - TSR$ della macchina tuttavia ci si può rendere conto che la macchina può fornire il valore richiesto in diverse condizioni (si guardi Fig. 1), che possono essere riassunte in tre condizioni, le prime due richiedono la modifica del TSR a cui la macchina opera quando viene sottoposta alle stesse condizioni di vento($TSR > TSR_{nom}$ $TSR < TSR_{nom}$) e, quindi, un cambio di velocità di rotazione del rotore, con possibili conseguenze sullo spettro dei carichi; la terza condizione è quella di mantenere lo stesso TSR (da cui il nome ISO-TSR), mantenendo quindi invariata la velocità di rotazione del rotore, dalla quale ci si attende un minore impatto dal punto di vista dello spettro dei carichi.

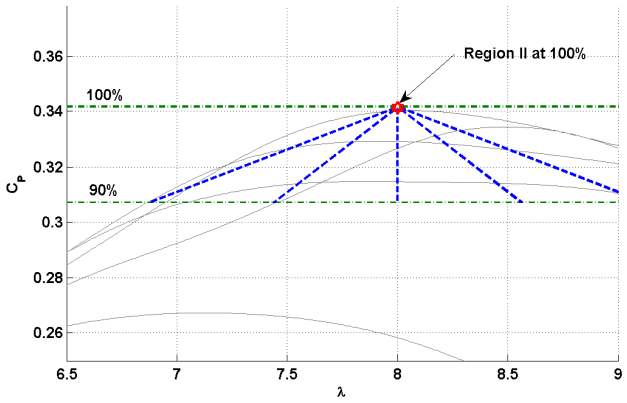

Figure 1: Regulation trajectory

La parzializzazione avviene quindi a TSR costante, prendendo i punti operativi che erano stati precedentemente calcolati per il controllo tradizionale e moltiplicandoli per un coefficiente riduttivo che esprima la percentuale di potenza che la macchina deve erogare. Il suddetto coefficiente moltiplicativo diventa quindi anche il set-point di potenza che la il controllore di wind farm invierà al controllore della macchina, la quale in maniera autonoma provvederà a regolarsi secondo l'istruzione ricevuta.

Il controllo del generatore non viene modificato, ma viene cambiata solo la traiettoria di regolazione della macchia in passo e coppia alla macchina

viene solo richiesto un valore diverso di coppia e di passo in funzione della parzializzazione richiesta. Alla macchina vengono fornite delle tabelle di set point per passo e coppia per un certo numero di parzializzazioni, fra le quali essa interpolerà per fornire il valore richiesto dal controllore di wind farm.

Dopo aver definito come avviene il controllo al livello "wind turbine", si passa poi alla spiegazione di come avviene la comunicazione fra il controllore di wind farm e quello della macchina. La comunicazione avviene grazie ad una libreria C che consente di codificare i protocolli di comuncazione fra un codice C e i sistemi di controllo delle macchine. Pertanto, il *Super-controller* è un codice scritto in linguaggio C, nella quale sono state realizzate delle funzioni che consentono la lettura e la scrittura di dati sul controllore stesso. Dal punto di vista fisico, il computer su cui viene eseguito il *Super-controller* è un PC tradizionale con sistema operativo Windows, e connesso alle macchine per mezzo di un hub Ethernet.

Successivamente, il capitolo si sofferma a descrivere in maniera dettagliata la logica di funzionamento del controllore, spiegando che esso implementa due modalità, una manuale, nella quale l'operatore può definire quale parzializzazione richiedere alla macchina attraverso un'interfaccia grafica ed una automatica nella quale è stato implementato un algoritmo di ottimizzazione che successivamente verrà descritto. Quando nessuna delle due manualità risulta attiva,il controllore di wind farm viene disattivato, lasciando che le macchine si regolino in maniera autonoma.

Nella modalità automatica è stato implementato un algoritmo di ottimizzazione di tipo "Simulated Anneling". Questo è un algoritmo metaeuristico per l'ottimizzazione globale di problemi non lineari. La sua peculiarità è quella di avere un parametro chiamato "temperatura" che diminuendo, riduce progressivamente la probabilità che vengano accettate delle soluzioni che non migliorano la cifra di merito, condizione necessaria ad evitare che l'algoritmo trovi un ottimo locale e non globale.

Il Capitolo 3 continua presentando il modo in cui è stato tarato l'algoritmo, e particolarmente il parametro "temperatura", che risulta essere quello più difficile da calibrare dal momento che la probabilità viene gestita da una funzione esponenziale della temperatura e del "salto" che la cifra di merito compie da un'iterazione all'altra.

Dopo aver dimostrato la convergenza dell'algoritmo attraverso un modello numerico, appositamente sviluppato basandosi sul modello di scia di Park, vengono presentati i risultati numerici e successivamente quelli sperimentali realizzati al banco prova.

I risultati sperimentali evidenziano che il controllore della macchina è in grado di inseguire delle traiettorie parzializzate ed è in grado di passare da una all'altra secondo un gradiente definito in fase di progettazione senza

nessun tipo di problema. Infine viene dimostrata la capacità del *Super-controller* di raggiungere il valore di parzializzazione ottima in un tempo di 10 minuti. Confermando quindi con successo la capacità del *Super-controller* e garantendo quindi la possibilità di effettuare dei test in galleria del vento con un modello perfettamente funzionante.

Non è stato possibile tuttavia realizzare le prove in galleria del vento in tempo utile a causa di un guasto avvenuto ad una delle due schede di condizionamento del segnale degli estensimetri che permettonono di misurare la coppia sul rotore. Senza il feedback degli estensimetri risulta impossibie realizzare il controllo in coppia e quindi controllare la macchina in galleria del vento. Tuttavia, i risultati ottenuti sul banco prova risultano essere di ottima qualità e dimostrano il funzionamento del controllore e, non appena verrà riparata la scheda, verrà programmata la prova in galleria del vento.

Nell'ultimo capitolo vengono riassunti i risultati ottenuti, vengono descritti gli sviluppi futuri di questo progetto e le modalità con cui verranno eseguite le prove in galleria, portando all'attenzione alcune considerazioni che andranno considerate effettuando la prova in galleria.

Chapter 1

Introduction

1.1 Wind energy

The increasing cost of all the energy products based on fossil fuels as well as to the increasing sensitivity from modern societies and political world for environmental issues, followed by ambitious objectives of gaseous pollutants reduction in the atmosphere, has forced the major industrial countries to diversify the sources for energy supply. In this overview, renewable energies and particularly wind energy is experiencing a moment of great expansion as one of the most competitive sources for energy supply, having every year a great increase in energy production as it is possible to see from Fig. 1.1 and Fig. 1.2.

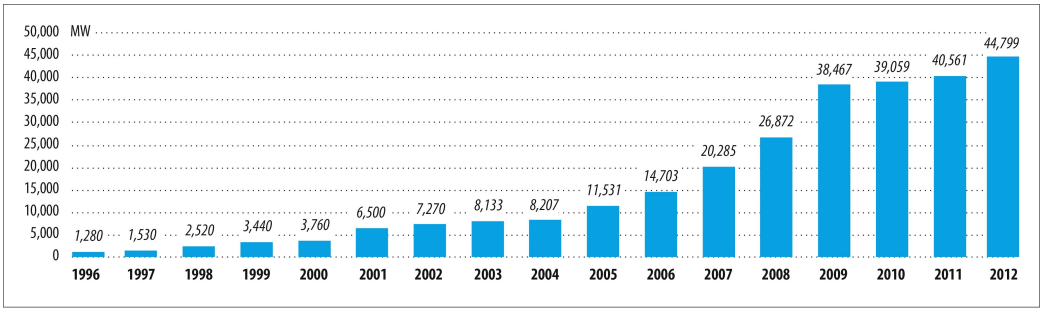

Figure 1.1: Global annual installed wind capacity 1996-2012 (source: GWEC)

In the last ten years the wind energy production has increased from 31 GW (2012) to 282 GW (2012), with China at the first place with a production of 75 GW. Italy is set at the fourth place in Europe and at the seventh in

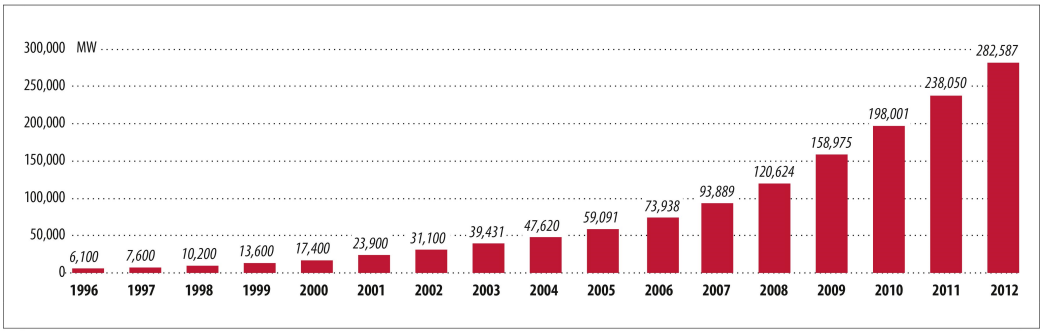

Figure 1.2: Global cumulative installed wind capacity 1996-2012 (source: GWEC)

the world with about 8 GW.

In this regard, the European Union (EU) has set the goal to achieve 20 % share of renewable energies in the overall energy consumption by 2020 and it is expected that wind energy will have a major role in achieving this target.

Until now, a huge effort has been made by companies operating in the wind sector and by national governments in terms of financial support to the research, whose contribution to innovation has allowed the development of even more efficient and high-tech wind turbines.

Furthermore, it is also quite clear as the final goal research and innovation should focus on, is to lower the cost of wind energy, which has become competitive when compared to the price of energy produced by traditional sources, like fossil fuels. However, the latter has not been reached yet and constant research and development is therefore needed.

1.2 Wind farms

At the present moment, wind energy production is principally organized in wind farms, that allows to reduce the required areas and that can be located onshore or offshore, with respective limits and advantages. Offshore wind is steadier and stronger than the on-land one and having less visual impact, but construction and maintenance costs are considerably higher. By contrast, onshore farms present opposite features: they have more visual impact, while construction and maintenance costs are lower.

As said, one of the most important target of research is the reduction of the cost of energy (CoE). There are various ways to reduce the cost of wind power production, for example: site selection, site layout(see [3] and [4]), optimal design, predictive maintenance and optimal control system design

(see [1]). In the past, most of the research has focused on stand-alone wind turbines, having the main purpose of increasing power production and reducing the loads experienced by the wind turbines, principally in order to reduce fatigue and extend the operative life of the machine (see ref [5], [6], [7], [8]).

Recent research has changed the target, working principally on wind farms performance, maximizing the total power production (instead of each individual one, which could be sub-optimal) and only a limited part includes load aspects in their objective functions, as explained for example: in [1], in [9], in [10], in [11], in [12], in [13], in [14], in [15] and in [16].

The development of a wind farm control can be justified by simple remarks that will be explained in the following.

Considering an actuator disc model of a wind turbine with stream tube boundaries shown in Fig. 1.3, given the far upwind wind velocity of V_∞ and the far downwind wind velocity V_d, it is possible to define the axial induction factor a as the parameter that describes the slowing of the wind speed between the free stream and the rotor plane:

$$a = \frac{V_\infty - V_{rotor}}{V_\infty} \tag{1.1}$$

The downwind wind speed is defined in Eq. 1.2:

$$V_d = V_\infty (1 - 2a) \tag{1.2}$$

So the power extracted by the actuator disc is given by eq 1.3

$$P = \frac{1}{2}\rho A V_\infty^2 4a \left(1 - a^2\right) \tag{1.3}$$

where A is the "swept area" of the rotor.

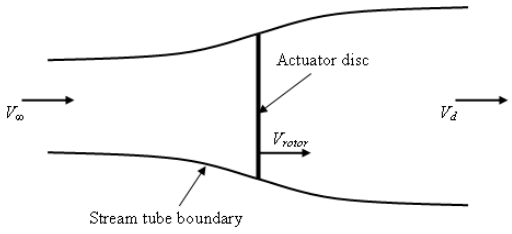

Figure 1.3: Actuator disc. The actuator disc describes the wind speed in proximity of an ideal wind turbine using the Momentum Theory

Considering a simplified wind farm, made up only of two wind turbines, in which one turbine is directly upwind to the other, it results immediately evident that a coordinate control of the wind farm is necessary. This simple

analysis assumes that wind turbines are far enough apart and that V_d is the value of both downwind wind velocity for the upwind turbine, and the upwind wind velocity for the downwind turbine. An isolated wind turbine maximize the extracted power with $a = \frac{1}{3}$. However, considering this value of axial induction factor in conjunction with Eq. 1.2 the downwind wind velocity for the upwind turbine results $V_d = \frac{1}{3}V_\infty$. By reducing a, $V_d$increases and the results of this simple analysis are represented in Fig. 1.4. In this graph, the power per unit of area is presented as a function of the axial induction factor. From this graph it is possible to see that $a = \frac{1}{3}$ doesn't represent the best condition, and that total power is maximized for $a = 0.2$

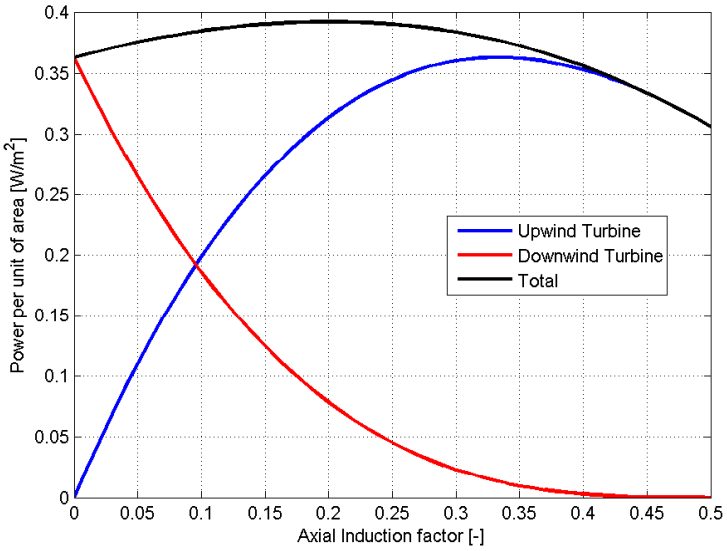

Figure 1.4: Power extracted from wind vs axial induction factor

These simple remarks hints that, through a wind farm control, decreasing the upstream wind turbine power, it is possible to increase the power production of the entire wind farm, and increasing wind farm power production, the CoE can be reduced and consequently wind energy becomes still more competitive.

At present, wind farm control is a relatively unexplored field and, as a results, literature presents a large number of approaches. Principally, the proposed methods change the control strategy, passing from individual and "greedy" control of the turbine to centralized algorithms which modify a base turbine algorithm to integrate it in an enhanced global performance.

Many studies focus the attention on realizing model based controllers, including in the objective functions complex mathematical models for wind turbines and for wake. However, the lack of models apt to describe the complete interaction dynamic of a large number of wind turbines leads to the idea

of realizing free-model controllers (see [11] [15]) or, as an alternative, controllers based on very simple models that describe only the main behaviour physical phenomenon.

In [16], a model based wind farm controller has been developed in order to optimize the loads and the power distribution. An optimizer takes into account the power produced by every single wind turbine and the loads operating on it, solves the optimization problem and sends back a new power set point to each wind turbine. The set point is then received by each wind turbine and its controller operates to maintain it. However, the author doesn't explain the control policy that the wind turbine controller follow to perform the power set point received.

In [11] a model-free controller is developed in order to maximize the total power output of a wind power plant by taking into account the wake effect. In this solution each wind turbine adapts its control settings on the informations that it receive from neighbouring turbines. The total power optimization is performed using a gradient-based optimization. Then, a comparison is made with the results obtained though the approach proposed in [15]. Even in this case, the authors don't explain how the wind turbine controller operates in order to perform the set point received.

Figure 1.5: Example of wake generated in a wind farm

Reference [15] proposes a model-free approach using game theoretic methods. In these references, Marden, Ruben and Pao showed a wind farm controller that aims to maximize the total power using a game theories, decentralizing the control from the wind turbines. Each turbine doesn't have

access to the functional form of the power generated by the wind farm and can't access the choices of other turbines.

Both [15] and [11] have based their studies basing on a largely diffused, extremely simple model of wake largely diffused: the *Park model* that will be fully presented and discussed in the following chapters. This mathematical model describes the effect of the wake as a wind speed deficit through simple geometrical considerations and thanks to its simplicity it is one of the most prevalent and studied model of wakes (for example see ref [17]).

The *Park model* is not the unique model present in literature. Indeed, a more complex example of mathematical wake model can be found in ref. [18], where a wind model, developed for studies on the dynamic interaction between wind farms and power system, is presented. As a conclusion, it is possible to realize that also wake models represent a challenging field in which constant research is required in order to obtain more reliable models, improving the results on wind farm controllers.

Eventually, it is important to highlight that the main benefits are obtained analysing the way turbines affect each other through their wakes and trying to reduce their intensity, adjusting blade pitch and generator torque (see [1] [15] [14] [16] [13] [3] [11] [12]), or, as an alternative, directing these wakes using yaw actuators to deflect the wake downstream of the rotor (see [10]).

1.3 The Approach

The great expansion that wind energy is experiencing offers the possibility to experiment a large number of solutions of different nature. In the last years, three principal kind of approach have been developed to test and study new wind farm controllers that will be presented and discussed in the following paragraphs.

The first one is realized on real wind turbines, using wind farms available to research. This approach represents the ideal case, having the advantage of using a real condition and inducing a real wake on other wind turbines. Nevertheless, the disadvantage is represented by the lacking of concrete possibility of testing wind farm control laws for research, principally because companies don't make available their wind farms for safety and economic reasons.

The second and most widespread approach is the use of numerical simulations, through advanced CFD codes or aeroelastic software (see [1], [6]). This approach gives the opportunity to obtain results simply through a computer, reducing the costs and the complexity of realizing a real or scaled

Figure 1.6: Hywind. The world's first full-scale floating wind turbine

wind turbine. However, the accuracy of these results must be verified and the ability of reproducing every feature of the physical phenomenon must be demonstrated. Particularly, the most important limit is given by the difficulty of reproducing in an accurate way wakes physical phenomena, because they are characterized by strong turbulence. Moreover, another important limit of this approach is the required time, a single test condition requires many hours and a sufficient computing power.

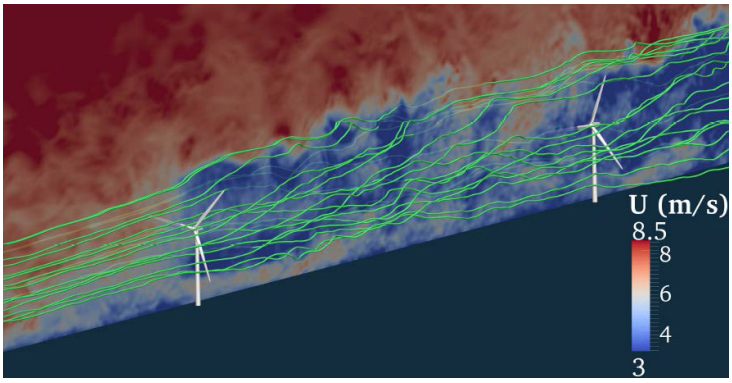

Figure 1.7: Example of numerical simulations. [1]

The third approach is represented by tests in the wind tunnels. This kind of approach is not as widespread as the numerical one, since an adequate structure is required and also because the scaling laws impose different limitations to the model: the mismatch between the Reynolds number of the

full scale wind turbine and the one of the scaled model, the difficulty of reproducing the elasticity of the structure of the wind turbine and the ability of reproducing in the wind tunnel the true conditions of the wind.

On the other hand, the advantages consist in having: lower costs, a better control, a major safety and, especially when the effects in a wind farm are studied, the opportunity to operate with real wake conditions and not with a wake based on a mathematical model.

Moreover, the wind tunnel tests also allow to modify wind farm configurations in less time, to operate with faster timescales and to develop a controller able to face problems similar to the ones affecting the full scale wind turbines.

The presented overview, as well as the availability of two wind turbine models developed by Politecnico di Milano in WT^2 project context has lead to the opportunity of developing a real time wind farm controller in order to start the study of wind farm control laws in the wind tunnel.

1.4 WT^2 Project

The WT^2 is a project developed by the Department of aerospace science and technology of Politecnico di Milano, sponsored by Vestas, world leader company in wind energy, with more than thirty years experience in wind turbine projects. The purpose of this project is the development of a multi Mega-watt wind turbine model in aero-elastic similitude, adequate for the wind tunnel experimentation.

The model aims to be a complementary element in the project phase of wind turbines, which, at the present moment, is based on several iterations between numerical simulations and 1:1 scale experimentation.

The actual approach principally shows two problems:

1. Uncertainty of the results of aero-elastic code, particularly in a case of extreme conditions, as defined by the norms.

2. Lack of experimental data in extreme conditions, caused by the exceptional nature of the phenomena.

Considering this overview, the development of models in aero-elastic similitude, adequate for wind tunnel experimentation, in a controlled and safe environment offers the opportunity to develop wind turbines control laws research and to reproduce those infrequent extreme conditions, otherwise difficult to be observed in a real contests.

The model realized is a scaled reproduction of Vestas V90, a 3MW wind turbine with horizontal axis and 90m rotor diameter. At the present moment, the Department has realized a second identical model, opening the opportunity to study and develop wind farm control laws.

1.5 Innovative content of the thesis

The innovative content of this work is the development of a controller able to perform a wind farm real-time control in the wind tunnel adopting a power set-point and simple to be integrated in a preexisting system.

The use of a simple power set-point allows to avoid the elaboration of complex mathematical models that lead to the possibility of approximating the physical phenomenon, by contrast, in this kind of approach the only error is given by the torque and rotor speed measures.

The versatility of this wind farm controller allows, in every moment, to change the optimization algorithm with another one and test it in the wind tunnel, on a real wind farm and with a real wake interaction.

The wind tunnel experimentation represents, at the present moment, a great opportunity for the wind energy research, but particularly for wind farm control research, indeed, in this environment it is possible to study the effects of a real wake generated by the upstream wind turbine on the downstream one and, for this reason, to obtain results more close to the full scale wind turbine, instead of mathematical models that are not able, at the present moment, to describe the complete physical phenomenon.

The wind tunnel experimentation of wind farms requires more reliable control solution, avoiding the study of such control solution that unattainable on real wind farm applications and allowing to face those problem that a theoretical study can't present.

1.6 Thesis Outline

The aim of this thesis work is the realization of a wind-farm super-controller, in order to maximize the total power produced by the two models V2 developed by Politecnico di Milano in the project WT^2, and the test of the controller in the wind tunnel environment.

The thesis is organized according to the following plan:

In chapter 2 the experimental set-up is presented. The wind tunnel environment is described, the V2 models are presented by the description of the onboard sensors, torque and pitch system, as well as the real-time control,

the model management system and the support tools that were designed for the testing, calibration and maintenance of the models.

In chapter 3, the author focuses more the attention on how the wind farm controller has been realized, starting from the stand-alone wind turbine control, describing how the stand-alone control has been integrated in the wind farm one, through the use of the "*ISO-TSR*" approach, developed to partialize the wind turbine power trajectory. Moreover, the chapter continues more practically, describing the wind farm controller, how the communication between the wind farm controller and the wind turbine one is performed and the control logic. Eventually, the chapter describes how this controller has been tested through the use of a simulated annealing algorithm, tuning the algorithm parameters through numerical simulations and finally testing it with test-bench simulations.

In chapter 4, the conclusions of this thesis work are presented, together with the limits and the strength points. Finally, the future developments of this work will be presented.

Chapter 2

The experimental set-up

In the chapter the tools and the experimental set-up that have been designed and used for the work will be described. In the first part, all the instrumentation required for the tests in the wind tunnel of Politecnico di Milano will be described. Afterwards, a complete description of the V2 models together with the support tools designed for test-bench and numerical tests are presented.

2.1 The wind tunnel

The GVPM [19] is the close circuit wind tunnel which has been used to perform all the tests of this project. The wind tunnel has two test sections: a low turbulence level test section, ideal for aerospace engineering applications, and a boundary layer large dimensions test section, built in the return tube, for civil engineering applications.

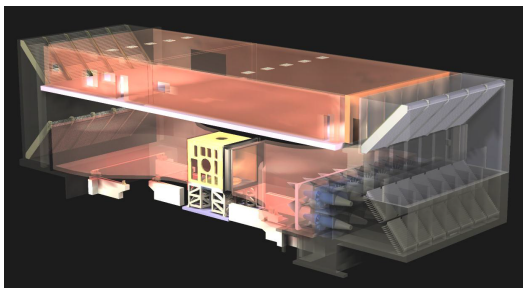

Figure 2.1: Plant configuration of the GVPM wind tunnel

The civil (boundary layer) test section (Fig. 2.2), is set on the second floor of the building, in the return tube and has an overall dimension of 3.84 x 13.84 x 36 [m] - respectively the height, width and length - that allows to

perform tests on very large models with low blockage effects and to reproduce atmospheric boundary conditions. In this section it is possible to achieve a maximum velocity of 14 $[m/s]$.

The aeronautical test section (Fig. 2.2) is placed at the ground height, it has a section area of 4 x 3.84 [m], that allows to achieve a maximum flow velocity of 55 $[m/s]$.

Figure 2.2: Civil (left) and aeronautical (right) test section details.

2.2 Wind turbine models

The wind turbine models used in this work are the results of the project WT^2 (1.4). They have been realized and developed at Politecnico di Milano in a three year-collaboration with VESTAS. The complex scaling criteria adopted during the project of these models have been fully described in ref [2] and lead to the scaling requirements reported in Tab. 2.1 .

Quantity	Scaling factor
Length	1 : 45
Time	1 : 22.84
Speed	1 : 1.97
Power	1 : 15477
Rotor speed	22.84 : 1
Torque	1 : 353574
Reynolds	1 : 88.64
Froude	11.6 : 1
Mach	1 : 1.97

Table 2.1: Scaling factors used for mapping the V90 into the model characteristics [2]

The scaling models, here named V2, will be briefly described in the following paragraphs.

2.2.1 General design

In Tab.2.2 the final dimensions of the models have been reported, adopting the scaling factors proposed in Tab.2.1

Quantity	Requirement
Rotor diameter [mm]	2000
Rotor tilt [deg]	6
Rotor cone [deg]	4
Rotor over-hang [mm]	≈ 80
Nacelle height [mm]	≈ 90
Nacelle width [mm]	≈ 90
Nacelle length [mm]	≈ 215
Spinner diameter [mm]	≈ 90
Tower height [mm]	≈ 1800

Table 2.2: Main dimensions of the scaled model [2]

2.2.1.1 Nacelle design

In Fig. 2.3 it is possible to observe the nacelle of the model. The main structural element of the nacelle is a rectangular carrying box, that provides the right stiffness to the entire nacelle group. Three electronic control boards (one for each actuator) are placed behind the box, welded on a flexible circuit and fixed to a triangular prism that rotates with the shaft. The electronic boards communicates with the control system thanks to a slip ring installed in backside of the nacelle.

The main shaft is mounted on two bearings and it was accurately designed to reproduce the 1^{st} in-plane collective rotor mode of the full-scale turbine.

The rotor azimuthal position is measured thanks to an optical encoder installed on the shaft. A three-axial accelerometer is fixed at the top of the tower measuring its accelerations. A double gear, with ratio reduction factor of two, allows the transmission of rotation between the shaft and the motor, positioned inside the top of the tower(Fig. 2.4). The motor provides the torque and it is connected to the gear through a flexible joint, balancing the 6 degrees of up-tilt. Finally a V90-similar nacelle cover is mechanically fixed above the carrying box to ensure a satisfactory wind flow quality.

2.2.1.2 Rotor and blade design

In Fig. 2.4 the final configuration of the rotor and blades layout is represented. The model rotor has been designed to allow the fastening of each

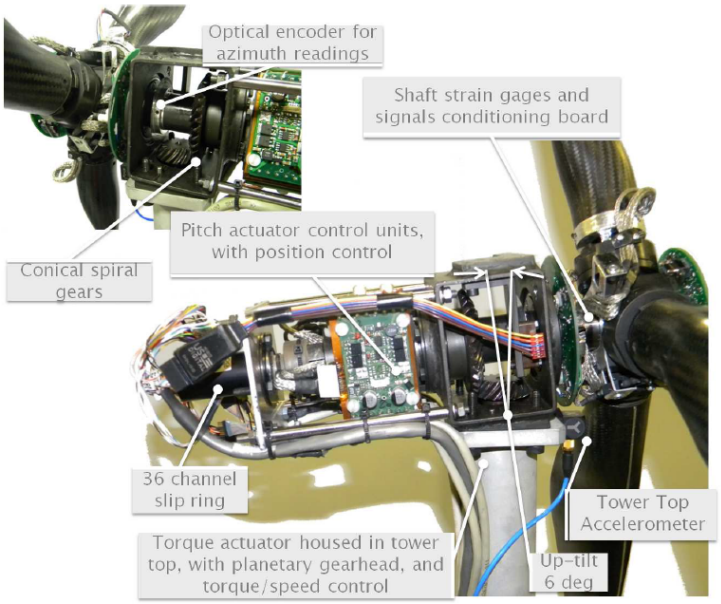

Figure 2.3: Nacelle arrangement

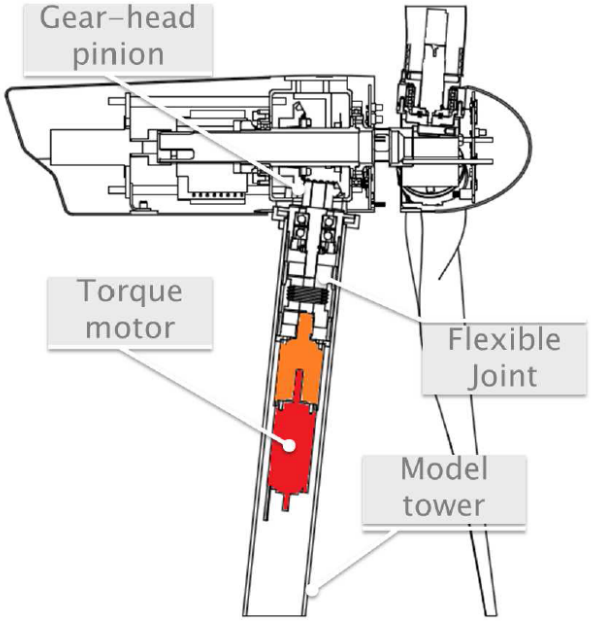

Figure 2.4: Scheme of torque transmission components

blade to the hub by means of a passing pin and, subsequently, the fixing of the entire rotor to the main shaft. This constructive solution ensures a rapid assembly of the rotor and permits to use both rigid or aero-elastic blades without changing the nacelle configuration.

Each blade hosts a pitch actuator with its relative built-in encoder. The gear head backlash (± 1 [deg]) of the selected pitch motor is removed using a torsional spring, which joints the blade root and the fixed-to-the-hub component. Another electronic board is placed in front of the rotor hub and provides power supply, conditioning and A/D conversion of the strain gauges bridges. Finally, a V90-similar spinner is mechanically fixed to the hub in order to ensure a satisfactory wind flow quality central rotor area.

2.2.1.3 Aerodynamics

The aerodynamic rotor design represented one of the key argument in the design process of the V2 model, in fact, in [2] an entire chapter was reserved to the aerodynamic description and to the identification process required to obtain reliable numerical results. The importance to the argument is due to the need of having a realistic aerodynamic performance of the model if compared to the multi-MW ones, principally in terms of power, thrust, and optimal TSR.

The optimal TSR constraint implies that the model should have the same solidity of the the reference rotor. For this reason it was decided to maintain the same chord distribution of the V90, with marginal modifications in the blade root region to take into account that the distance between the model hub center and the blade root is slightly greater than the V90 scaled one.

The choice of the airfoil was driven by the great mismatch between the Reynolds number, which in V90 is about $4 \div 5 \cdot 10^6$ while in V2 is $5 \div 6 \cdot 10^4$. In the past years a large number of research studies were conduced on aerodynamics at Reynolds number lower than 10^5, with great benefits in a large number of applications.

Much literature search was then carried out to identify the profiles to be used, and the choice cast on the profiles AH79-100C and WM006, whose shape is reported in Fig 2.5.

Particularly, the airfoil AH79-100C was used in the inboard section for $\eta = r/R \in [0.137, 0.423]$, while WM006 in the outboard one for $\eta \in [0.654, 1]$. Interpolations of the cross sectional shapes were limited to a relatively small transition region between the inboard and outboard sections, i.e. for $\eta \in [0.423; 0.654]$, and at the root region to smoothly deform the inboard airfoil into the blade root cylinder.

In [2], after having designed the model blade and identified the method to

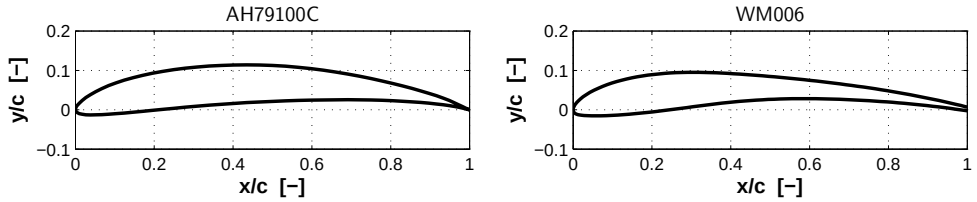

Figure 2.5: Model airfoils shape.

correct the aerodynamic performance from the wall blockage effects, a tool to identify the blade airfoils polar directly from experimental tests was developed. Indeed, not negligible deviations were expected between the estimated and measured rotor performance. Particularly, real airfoils polar could be different from the estimated ones due to:

- Uncertainties on real blade shape: in the outer region of the blade, chord is extremely small, for this reason, it is difficult to manufacture a composite-made blade with the correct desired shape, due to molds machining tolerances as well as to the unavoidable manual edging;
- X–foil poor capability to predict, with good accuracy, the polar data at low Re, specially with forced transition;
- Effectiveness of the designed strips in inducing the transition, and their effect on the aerodynamic characteristics.

Thanks to the identification tools explained in [2], it was possible to use the identified airfoils polar data to improve the ability of the `Cp-Lambda` code to predict the behaviour of the V2 model airfoil, obtaining numerical results more close to the experimental ones.

2.2.1.4 Tower design

The tower was designed so that the first fore-aft and side-side natural frequencies of the model match the scaled ones of the real wind turbine. This result was obtained opportunely projecting the thickness distribution of the tower, keeping in mind the constraint of having an external diameter as closed as possible to the V90 scaled one. This constraint allows to capture the principal aerodynamic interference between tower and rotor. The tower is mounted on a balance capable of measuring the three force and three moment components acting at the tower base. Finally, compressed air is blown in at the tower foot to cool the torque motor before escaping from a small hole in the back part of the tower top.

2.2.1.5 Sensors

The installed sensors are the ones necessary for the traditional control of a multi-MW wind turbine. The data coming from the sensors available on board are collected by the control system. They are used by closed loop control algorithms which drive the actuators and by the supervisory system that manages the possible machine states and handles emergencies. The model is equipped with:

- Sensors for measuring the pitch angle of every blade with ± 0.2 [deg] accuracy.
- An optical encoder for azimuth angle measuring, in order to allow testing of individual pitch control algorithms. The azimuth data are also used to get the rotor speed through numerical derivation;
- A three-axial accelerometer that measures the tower fore-aft and side-side accelerations. These data are used for monitoring purposes and can also be used as feed-back signals by control algorithms that actively dampen the tower oscillations.
- Strain gauges for measuring the stresses acting on the tower, the main shaft and the blades; these are the most commonly used measures for control purpose.
- A balance, positioned at the tower base, to measure the three forces and three moment components acting at the tower base.
- Two Pt100 probes are used for monitoring the winding and gear head temperature of the torque actuator, with the supervisory system programmed to change the model state from POWER PRODUCTION to IDLING condition in case of generator overheating.

2.2.1.6 Actuators and control

The requirements on actuators characteristics were derived from the direct application of the scaling laws on the V90 technical data related to the actuation subsystem. The model is equipped with:

- A torque actuator positioned inside the tower
- Three pitch actuator positioned inside the blade root.

Torque control

Torque actuation is realized through a Maxon brushless motor EC-4-Pole-30BL-200W, selected for its characteristics, i.e. rotational speed up to 400[rpm], dimension compatible with space available at the top of the tower and a maximum power similar to the scaled one of the full scale system. The motor can also operate as a generator and the produced electrical power dissipated by a 12-75V/5.0 [Ω] Shunt Regulator chopper, connected to an external 6.8 [Ω] resistance, which allows to dissipate a continuous power up to 300 [W].

The actuator can be controlled in speed or in torque mode. Speed control is performed using the motor encoder measure as feed-back signal and sending the desired reference speed to the electronic control using a Can-open communication protocol at data transfer speed of 500[kb/s]. The gains of the 4-Q-EC-DES-50/5 internal PI speed controller were appropriately tuned to achieve a good speed reference tracking with low level of speed and current oscillations.

Usually, in small size wind tunnel model, torque control is realized in open-loop, taking advantage from the well-known relationship present between Torque and current $T = K_Q i$. However, in V2 model, there are several difficulties attending:

- Rotor speed varies depending on the system operating region
- Temperature is subject to considerable variations during operation, being the motor used at the limit of its capacity
- Nacelle bearings and gear-head provide variable and difficult to predict friction torques

Having considered all these complications, during the project it was developed a closed-loop on torque, implemented on Bachmann M1 real-time system whose output is a current reference sent to the motor electronic control.

The need of a fast response of the system lead to oscillations of considerable magnitude. The suppression of these oscillations was provided with a feed-forward (Fig. 2.6), that allowed disturbance rejection without limiting the controller speed.

Pitch control

Pitch actuation is performed with the Faulhaber brushed motor 1724T0 18SR, that provides accuracy and repeatability of pitch positioning, a dimension compatible with the housing space available in the blade root, a maximum pitch rate high enough to allow emergency shut down operations

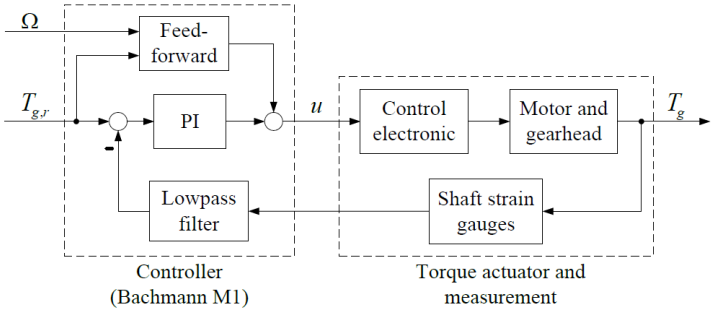

Figure 2.6: Torque control loop.

and a bandwidth sufficiently wide to ensure individual pitch control capability.

Each pitch actuator is driven by its own control board and all the three control boards are nodes of the same Control Area Network (`CAN`) using a `Can-open` communication protocol at data transfer speed of 500[kb/s].

2.2.2 Real-time supervisor

The model is equipped with a hard-real-time system, capable of acquiring the readings of all the installed sensors on the model, as well as the data related to the wind tunnel environment, it and uses them to apply sophisticated control algorithms sending output set points to the actuators, reproducing a supervisor as closed as possible to the real wind turbine one.

Every 4 [ms], the `M1-CPU` takes all the sensors reading inputs and sends as outputs pitch and torque demands to to the actuators.

2.2.2.1 Model state machine

Every real wind turbine is managed by a supervisor that is able to switch through different states of the machine basing on the operational conditions or situations (start-up, energy production, emergency, etc.). The logic operating on the scaled model, resumed in Fig. 2.7, represents an augmented version of the one implemented in a real machine, since it is necessary to handle additional operating conditions.

At the beginning of each test, the machine changes from IDLING, with all actuators disabled, to the state of FUNCTIONALITY TESTING, where the correct functioning of the model is verified and followed by the zero setting of the sensors readings and pitch actuators encoders. If the model check is successful, the state is changed to PARKING and the wind turbine operates in standing still condition. Successively, the user can decide to operate

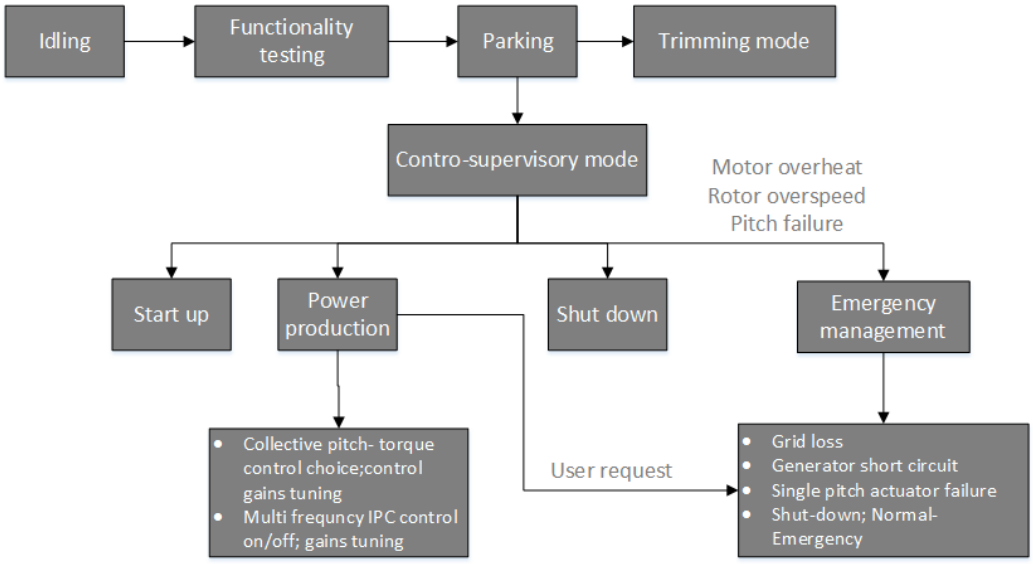

Figure 2.7: Implemented model state machine.

the model in TRIMMING MODE, usually used for aerodynamic focused tests since it is possible to regulate the machine at user-defined values of rotor speed and blade pitch, or in CONTROL-SUPERVISORY MODE. Here the supervisor switches among the machine states of START UP, POWER PRODUCTION, SHUT DOWN and EMERGENCY MANAGEMENT in an autonomous way, e.g. for managing start up and shut down procedures on the basis of the measured rotor speed and in case of real emergencies (like an excessive rotor speed or overheating of the torque actuator), or by the intervention of the user, e.g. for reproducing an extreme condition like an emergency shut down with grid loss. In POWER PRODUCTION state it is possible to switch among different collective pitch-torque control laws, whose gains can also be changed by the users during the wind tunnel testing, and to enable/disable multi-frequency individual pitch control capabilities, with the possibility, also in this case, to tune as desired the controller gains.

An operator control station implements software for the management of the experiment, for the data logging and visualization of all measurements through the support of dedicated graphical interfaces (as that reported in Fig 2.8), which allowed to switch between the machine states, enable and disable the desired controller and tune the controller gains.

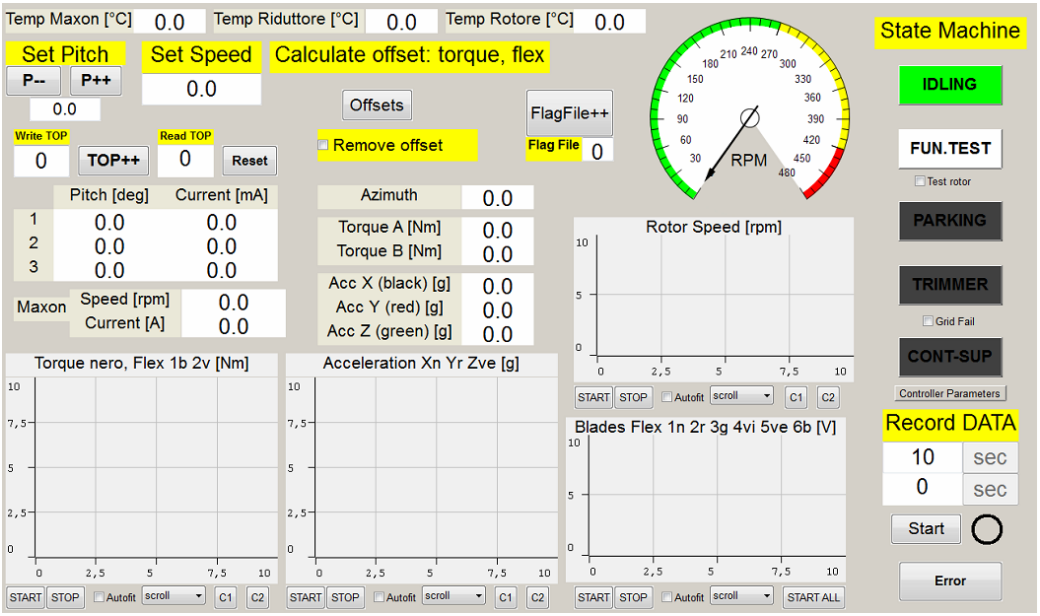

Figure 2.8: Graphical interface for the model management

2.2.3 Support tools

Finally, the wind turbine model is equipped with several support tools for its testing, calibration and maintenance. The most important tool is a back-to-back test bench (Fig. 2.9), in which blades are replaced with cylinders that allow to reproduce real rotor inertia. It was used for the hardware-in-the-loop test of the control-supervisory algorithms. The aerodynamic torque was provided by a brushless motor `Maxon EC-45`.

The relation between the gear-head output shaft torque and the motor current-rotor speed was experimentally estimated, while the required aerodynamic torque $T_{a,r}$ is real-time computed using, as input, the pitch and rotor speed read with the nacelle sensors, the rotor aerodynamic torque coefficients $C_T(\beta;\Omega)$ and an user defined time history of the wind speed, as shown in Fig.2.10.

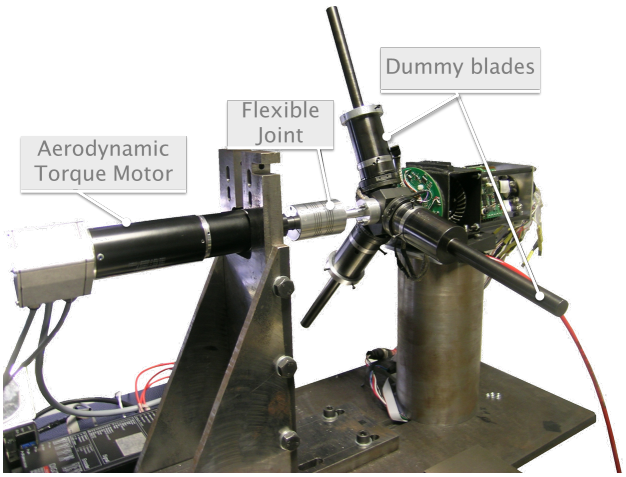

Figure 2.9: Test bench

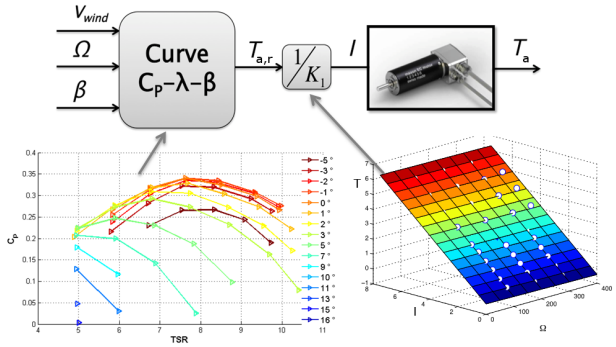

Figure 2.10: Aerodynamic torque computation.

2.2.4 Simulation tools

All the numerical simulations realized during the development of the wind farm control have been supported by the comprehensive aero-elastic simulation environment (Fig. 2.11) `Cp-Lambda` (Code for Performance, Loads and Aeroelasticity by Multi-Body Dynamic Analysis [20]).

`Cp-Lambda` is based on a multibody approach, which is characterized by the full finite-element method, i.e. no modal-based reduction is performed on the deformable components of the structure. Cartesian coordinates are used for the description of all entities in the model, and all degrees of freedom are referred to a single inertial frame; the formulation handles arbitrarily large three-dimensional rotations.

The turbine blades and tower are modelled using geometrically exact, composite-ready beams. The formulation models beams of arbitrary geometry, including curved and twisted reference lines, and accounts for axial,

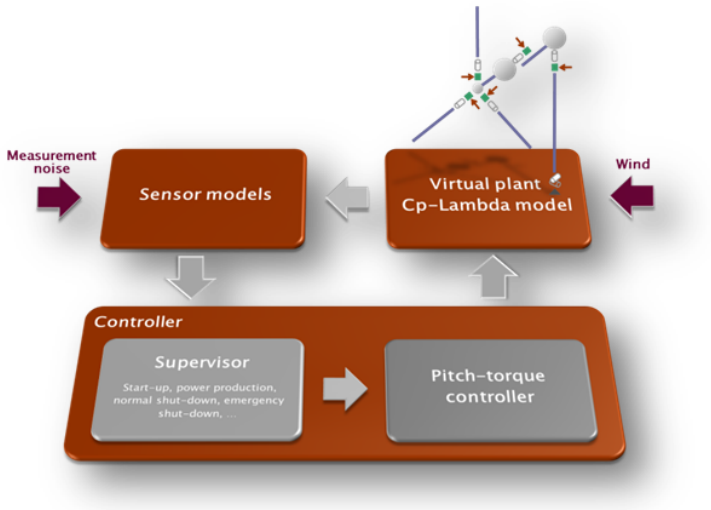

Figure 2.11: Multi-body aero-servo-elastic simulation tool.

shear, bending, and torsional stiffness. Joints are modeled through holonomic or nonholonomic constraints, as appropriate and all joints can be equipped with internal springs, dampers, backlash, and friction models.

The lifting lines are based on classical two-dimensional blade element theory, and account for the aerodynamic center offset, twist, sweep, and unsteady corrections. At a number of span-wise stations along each lifting line, the aerodynamic characteristics of the airfoil used at that location are given using look-up tables, which store for a given number of angles of attack and Reynolds numbers the values of the sectional lift, drag and moment coefficients. Through the appropriate definition of these coefficients one can also model those aerodynamic phenomena related to 3D flow bahaviour, such as the stall delay in the inner part of the blade due to Coriolis accelerations. Lifting lines are used here to model the aerodynamic characteristics of the blades, but also of the tower and of the nacelle. The code implements the Peters-He dynamic inflow wake model and a classical blade-element momentum (BEM) model based on the annular stream-tube theory with wake swirl. Tip and hub loss models are also considered.

Wind is modelled as the sum of a steady state mean wind and a perturbation wind, accounting for turbulence and/or gusts. The deterministic component of the wind field implements the transients specified by IEC 61400, the exponential and logarithmic wind shear models, and the tower shadow effects, which include the potential flow model for a conical tower, the downwind empirical model of Powles, or an interpolation of these two models. The stochastic component of the wind field is precomputed before

the beginning of the simulation for an assigned duration of time and for a user-specified two-dimensional grid of points.

The user can specify a number of sensors on the virtual prototype of the turbine, which provide output information for the analysis. The same sensor outputs can also be fed as inputs to the onboard controllers, which, in turn, operate the system actuators. Controllers, which can include supervision logics and feedback controllers, are implemented as user-defined routines that are linked with the rest of the code. The code supports static and transient analysis, and the computation of eigenfrequencies and eigenmodes about deformed equilibrium configurations. Finally, the model preparation and data interpretation phases are supported by various graphic procedures, including animations and time history plots, while automated procedures support a number of standard operations, such the computation of Campbell diagrams, the generation of C_P vs. tip-speed-ratio curves, the tracing of power curves, the determination of ultimate loads and fatigue equivalent loads using rain-flow analysis, etc.

The full scale mathematical model is based on data provided by the sponsor, while the mathematical model of the scaled wind turbine is based on its measured geometric, structural and aerodynamic properties. In particular, the model structural properties were computed using:

- well known analytical formulas for tower properties calculation;
- composite blade analysis code ANBA (Anisotropic Beam Analysis) for computing the cross sectional characteristics of the blade, verified with detailed three-dimensional FEM models and corrected with the aid of identification techniques when necessary;
- detailed three-dimensional FEM computation for the main shaft and the nacelle properties calculation.

The masses of the model were updated according to data obtained by precise weighing, allowing the modelling of all non-structural masses, such as wiring and aerodynamic covers.

The reliability of model aerodynamic data is proved thanks to identification results, while the actuators dynamic and range, as well as the sensors and control, faithfully reproduce what is available on the real model.

Chapter 3

Wind farm control development

The main purpose of the present chapter is the description of the wind farm regulation policy and control and its implementation on the two V2 models available from the project WT^2.

In the first part of the chapter, the classic regulation trajectory is described, after that, the author continues describing the way the wind turbine has been modified in order to reduce the effects of the wake on the downstream wind turbine and so improving the total power production. Eventually, the chapter describes the way the wind farm controller has been developed, describing how the communication between wind farm and wind turbine controller has been realized and its functioning logic.

The second part of the chapter describes the optimization algorithm that have been implemented on the wind farm controller and how it operates in order optimize total power production. In this part of the chapter, the simulated annealing algorithm together with its limits and its advantages is presented, after that the chapter describes how the algorithm parameters have been calibrated reproducing the wake with the "*Park wake model*" as mathematical model.

Eventually, the chapter ends describing the tests that have been performed on the test bench to validate the controller developed before the tests in the wind tunnel.

3.1 Stand-alone wind turbine control

3.1.1 Regulation policy

The regulations of variable speed wind turbines are made according to different control laws, depending on the intensity of the mean wind speed. It is possible to identify three different power production regimes: region II, II½

and III, plus two regions of non-production: region I and IV.

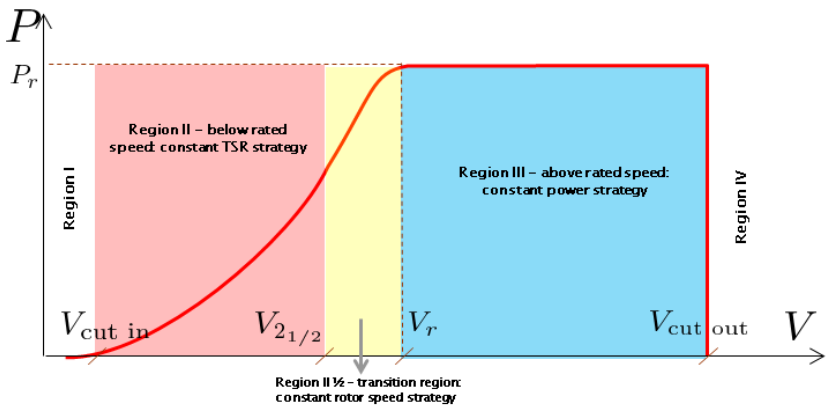

Figure 3.1: Traditional regulation policy.

Region I and IV are the conditions in which the mean wind speed is respectively lower than the cut-in speed or higher than the cut-out wind speed. In region I it is not convenient to start the energy production, so the wind turbine is kept in an idling condition. In Region IV wind speed is too high, and to reduce loads on the structure the wind turbine is kept in an idling condition.

The first regime of production is called region II, here power is maximized operating at the maximum value of power coefficient (C_P) and Tip Speed Ratio (TSR) is kept constant for all wind speed. Blade pitch is fixed to the value that maximizes the power coefficient and electrical torque is regulated so as to trim the machine at the desired rotor speed.

Power is expressed as:

$$P^{II} = \frac{1}{2}\rho A V^3 C_P(\lambda^{II}, \beta^{II}) \tag{3.1}$$

for what it was previously said, in Region II it is possible to express some of the terms present in Eq.3.1 as follows:

$$C_P^{II} = \max C_P(\lambda, \beta) \tag{3.2}$$

$$\lambda^{II}, \beta^{II} = \arg\max_{\lambda,\beta} C_P(\lambda, \beta) \tag{3.3}$$

So, in Region II, λ and β are kept constant and rotor speed increases as a linear function of the wind speed.

$$\Omega^{II}(V) = \frac{\lambda^{II}}{R} V \tag{3.4}$$

and considering Eq. 3.1, Torque can be expressed as:

$$T^{II} = \frac{P^{II}}{\Omega^{II}} \rightarrow T^{II}(V) = \frac{1}{2}\rho A R V^2 \frac{C_P^{II}}{\lambda^{II}} \tag{3.5}$$

Region II½ is introduced only in presence of a blade tip speed constraint, and it extends from the speed at which the blade tip reach the speed constraint ($V_{II^{1}/_{2}}$) to the speed at which power rated is reached (V_r), called rated speed.

In this region, power is still lower than the rated value, while a constant rotor speed policy must be applied in order to respect the tip speed constraint, for this reason the controller has to operate maximizing the power coefficient keeping rotor speed constant.

However, considering Eq. 3.6:

$$\lambda^{II^{1}/_{2}}(V) = \frac{\Omega_{r,t} R}{V} \tag{3.6}$$

If Ω is kept constant and wind speed increases, λ decreases, for this reason, until rated power is reached, the controller has to change β in order to maximize the power coefficient and consequently power.

So it is possible to define:

$$\beta^{II^{1}/_{2}}(V) = \arg\max_{\lambda,\beta} C_P(\lambda^{II^{1}/_{2}}, \beta) \tag{3.7}$$

and finally

$$T^{II^{1}/_{2}}(V) = \frac{1}{2}\rho A V^2 C_P(\lambda^{II^{1}/_{2}}, \beta^{II^{1}/_{2}}) \tag{3.8}$$

Note that in Region II½ the rotor speed is set to $\Omega_{r,t}$, which is not the rated rotor speed (Ω_r), a complete explanation of the difference between the two terms will be given in the following paragraph.

Region III starts when rated power is reached, here the control switch to constant power control policy until the mean wind speed exceeds the cut-out value, where the machine is shut down. In this region of production, as power and rotor speed are kept constant, TSR changes as $\lambda^{III}(V) = \frac{\Omega_r R}{V}$ while torque is kept constant at the rated value. It results that C_P has to change in order to make the wind turbine producing rated power, as well as the pitch angle is increased seeking at the equilibrium between electrical and aerodynamic power. Considering Eq. 3.1 and defining C_{P_r} and λ_r respectively as the power coefficient and Tip Speed Ratio values at which rated power is reached, it is possible to express C_P^{III} as described in Eq. 3.9:

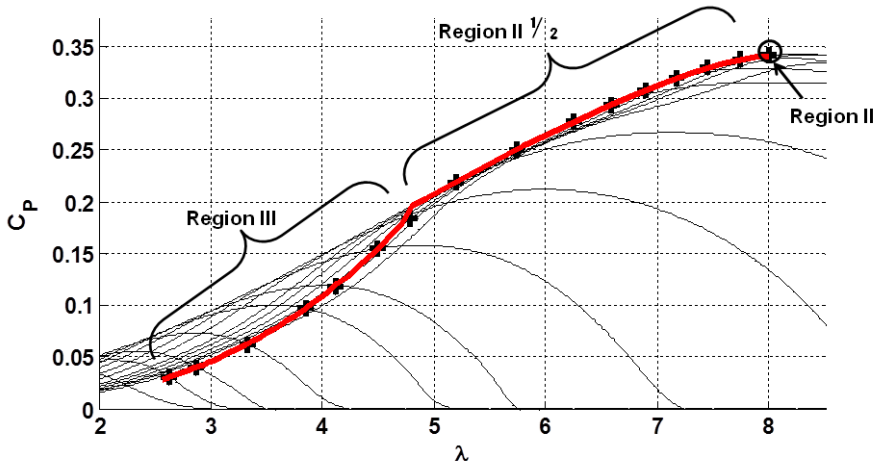

Figure 3.2: Traditional control on C_P vs TSR

$$C_P^{III} = C_{P_r} \left(\frac{\lambda^{III}}{\lambda_r} \right)^3 \tag{3.9}$$

while the blade pitch is:

$$\beta^{III} \text{ such that} : C_P(\lambda^{III}, \beta) - C_P^{III} = 0 \tag{3.10}$$

The regulation policy is shown in Fig. 3.2, where it is plotted over the $C_P - \beta - \lambda$ curves. Its formulation is also resumed in Tab. 3.1.

	Region II	Region II½	Region III
$\lambda_{ref}(V)$	$\arg\max_{\lambda} C_P(\lambda, \beta)$	$\frac{\Omega_{r,t} R}{V}$	$\frac{\Omega_r R}{V}$
$\Omega_{ref}(V)$	$\frac{\lambda}{R} V$	$\Omega_{r,t}$	Ω_r
$\beta_{ref}(V)$	$\arg\max_{\beta} C_P(\lambda, \beta)$	$\arg\max_{\beta} C_P(\lambda^{II1/2}, \beta)$	β such that: $C_P\left(\lambda^{III}, \beta\right) - C_{P_r}\left(\frac{\lambda^{III}}{\lambda_r}\right)^3 = 0$
$T_{ref}(V)$	$\frac{1}{2}\rho A R V^2 \frac{\max C_P(\lambda,\beta)}{\lambda^{II}}$	$\frac{1}{2}\rho A R V^2 \frac{\max C_P\left(\lambda^{II1/2},\beta\right)}{\lambda^{II1/2}}$	$\frac{P_r}{\Omega_r}$

Table 3.1: Regulation policy resume

3.1.2 Control

Once defined the machine regulation policy, starting from experimental or numerical characterization of the rotor performance ($C_P - \lambda - \beta$ curves), it is possible to trace the schedules of the optimal regulation set points for the rotor speed collective blade pitch and generator torque (see Fig. 3.3).

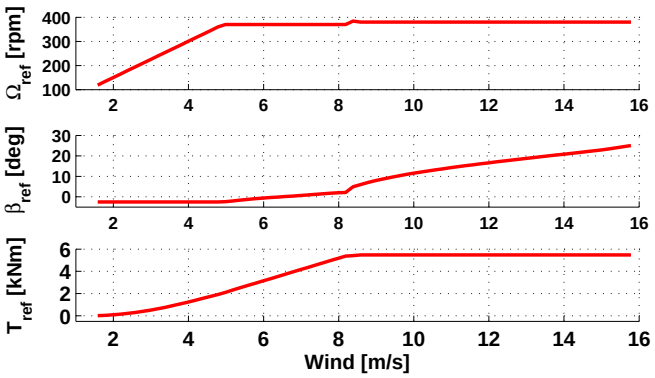

Figure 3.3: V2 model control trajectories

The goal of the wind turbine control system is to track the regulation set points by changing the actuators outputs. To this aim, two PI controllers have been implemented within the V2 real-time hardware: one controller tracks the torque set-point, while the other one tracks the pitch set-point.

The demanded torque value T_{dem} is computed by torque controller on the base of Eq. 3.11, i.e. looking at the maximum between the optimal region II torque T^{II} and the output of the PI controller T_{PI}.

$$T_{dem} = \max \begin{cases} T^{II}(\Omega) = \frac{1}{2}\rho\pi R^5 \frac{C_P^{II}}{(\lambda^{II})^2}\Omega^2 \\ T_{PI} = K_{P_T}(\Omega - \Omega_{r,t}) + K_{I_T}\int(\Omega - \Omega_{r,t}) \end{cases} \tag{3.11}$$

How torque control works can be easily explained: in region II the rotor speed remains lower than its reference value, so T^{II} results higher than T_{PI} and it results $T_{dem} = T^{II}$. By contrast, in high wind speed conditions, rotor speed can be higher than its reference. In this case, T_{PI} is higher than region II torque and therefore it determines the demanded torque value. Anti-windup technique is implemented in order to avoid negative effects due to switching logic, as well as controller output is limited in the range $T \in [0, \frac{P_r}{\Omega_r}]$.

Blade pitch demand is also computed by means of the PI controller of Eq. 3.12.

$$\beta_{dem} = k_P \left(\Omega - \Omega_r\right) + k_I \int_{t-t_i}^{t} \left(\Omega - \Omega_r\right) d\tau, \tag{3.12}$$

where the rotor speed measure and the rated speed are respectively used as feedback and reference values. Similarly to torque controller, actuation limits are also implemented together with anti-windup techniques; in particular, a lower limit, i.e the minimal allowable pitch angle, is defined and scheduled as function of wind speed and it is showed in Fig. 3.4. In the figure, it is possible to observe that in Region II and II1/2 β_{ref} and β_{min} are completely overlapped, by contrast, in Region III their values diverge. It is important to remark that torque and pitch controllers do not have exactly the same reference values. Indeed, the reference for the pitch controller is set equal to the rated rotor speed (Ω_r), while the reference for the torque controller is set on a slightly lower value ($\Omega_{r,t}$). This small gap is by itself sufficient to eliminate unnecessary pitch action in region II1/2 and unnecessary torque action in region III.

Both pitch and torque controls are active in all operating regions, however, thanks to its implementation, when the first is saturated, the other one is actively controlling the wind turbine and viceversa.

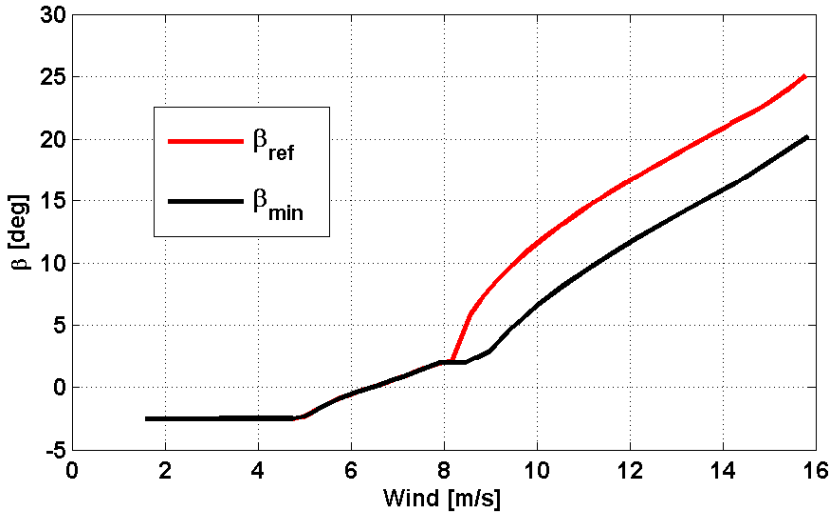

Figure 3.4: Comparison between β_{ref}, given by the regulation trajectory and β_{min}, introduced as anti-windup technique.

3.2 Wind turbine control for wind-farm control application

In most cases, the wind farm control problems are approached formulating them as optimization problems in which the cost function is the total power production, while, only few research studies (for example [14] and [16]) include also the loads in the cost function. Literature presents also different solutions in the choice of the optimization variables, for example, [15] proposes a solution in which the optimization variables are the axial induction factors that every wind turbine has to provide, while in [16] the optimization variables are the power set-points for each wind turbine.

Despite the differences present in the choice of the optimization variables, all the references proposed share the idea that, to improve the total power production of a wind farm, it is necessary to reduce the power produced by the upstream wind turbines in order to reduce the effects of the wake on the downstream ones.

First of all, it is necessary to highlight that, in a real wind farm, it is difficult to adopt a solution like that one used in [15]. Indeed, citing [21], the axial induction factor is defined as:

> the fractional decrease in wind velocity between the free stream and the rotor plane.

It is immediately self-evident that the axial induction factor can hardly be measured on the field and has to be estimated through a mathematical model, leading to a procedure subject to possible errors. In a large number of examples available in literature the axial induction factor is linked to C_P making use of extremely simplified mathematical models, that are unable to describe the complete physical phenomenon and lead to significant errors and approximate optimal solutions. By contrast, power can be simply measured and doesn't require the support of any mathematical model, reducing the probability of committing errors in power computing.

By considering the proposed overview and the experimental nature of the present work, the axial set-point approach has been discarded to the benefit of a power set-point approach.

In order to reduce the power, the power equation was considered:

$$P = \frac{1}{2}\rho A V^3 C_P(\lambda, \beta) \tag{3.13}$$

given that the air density ρ, the rotor area A and the wind speed V can not be affected by the controller, it is self-evident that the wind turbine

controller can only modify the C_P. Therefore, the only way to reduce wind turbine power is asking to the wind turbine to perform a lower C_P, i.e. extracting from the wind only a partial part of the available power. This procedure is here called *partialization*.

In Fig. 3.5 a zoom of the top of $C_P - \beta - \lambda$ curves, obtained through the numerical simulation tool (§2.2.4), has been represented. In the figure, the maximum C_P value, the same value multiplied by the coefficient 0.9 (90% of the available power) and the Region II operative point were highlighted. It is possible to see that, at 100 % of the available power, the Region II operating point is univocally defined (it is the maximum C_P value); however, operating at 90 % of the available power means that every single point lying on the intersection between the 90 % line and the $C_P - \beta - \lambda$ curves represents a possible operating condition. By considering all the these possible operating points, it is possible to distinguish three different operative strategies, resumed in Tab. 3.2.

1^{st} condition	2^{nd} condition	3^{rd} condition
$\lambda^{II}_{90\%} < \lambda^{II}_{100\%}$	$\lambda^{II}_{90\%} = \lambda^{II}_{100\%}$	$\lambda^{II}_{90\%} > \lambda^{II}_{100\%}$
$\Omega^{II}_{90\%} < \Omega^{II}_{100\%}$	$\Omega^{II}_{90\%} = \Omega^{II}_{100\%}$	$\Omega^{II}_{90\%} < \Omega^{II}_{100\%}$

Table 3.2: Possible operative conditions at 90% of the available power

The first strategy is the case in which TSR is lower than the one at 100% of the available power. By considering to operate at same wind condition, reducing TSR means to reduce rotor speed; by contrast, the third strategy is the case in which TSR is higher than the one at 100 %, and so rotor speed has to increase. Despite their differences, in both cases it is necessary to change the rotor speed, with possible impact on load spectra.

The second strategy consists on keeping the TSR constant, i.e. rotor speed doesn't change under constant wind condition; it is expected that this startegy could have a lower impact on the load spectra, but further investigation are required. However, the main advantages of this strategy are that it requires the definition of only one *partialization* parameter and it allows to use the control described in §3.1. For these reasons, this approach, here called *"ISO-TSR"*, has been chosen as control strategy and it will be fully described and examined in the following paragraphs.

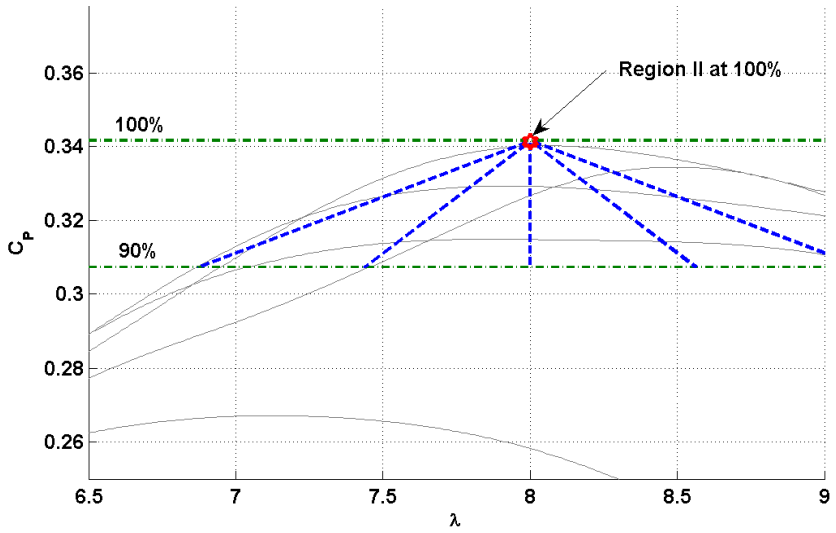

Figure 3.5: Regulation trajectory: ISO-TSR approach explaining

3.2.1 The *ISO-TSR* approach

Given that both full-power and partial-regulated wind turbines operate at same TSR, the partialized $C_p - \lambda$ regulation curve, i.e. how C_P changes as function of TSR, can be easily obtained scaling down the full-power $C_p - \lambda$ curve by a coefficient $0 < p < 1$, which represents the amount of requested power expressed in fraction of the available one. Fig.3.6 shows the partialized $C_p - \lambda$ regulation curves for several partialization factors p.

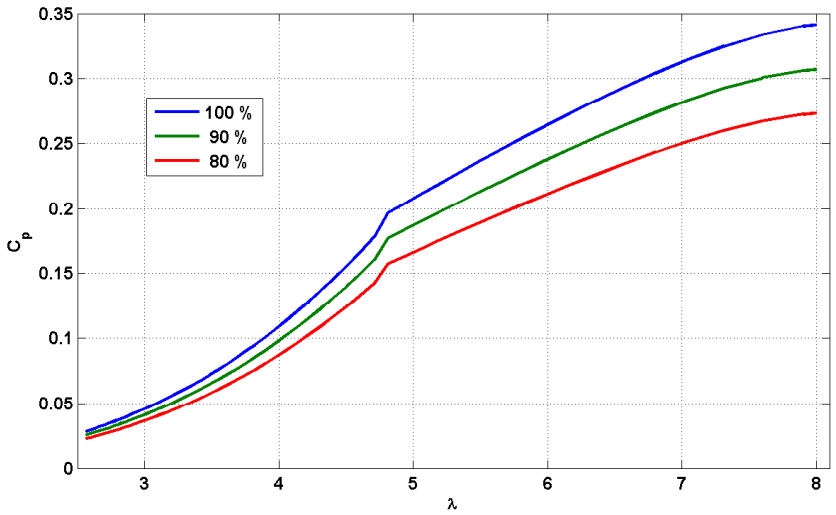

Figure 3.6: Partialized $C_p - \lambda$ curves for several partialization factors p

The regulation policies for a partial-regulated machine can be also easily computed. Indeed, the rotor speed is the same of the full-power machine, the torque is scaled down of the partialization factor p, while the blade pitch is computed by seeking the equilibrium between electrical and aerodynamic power. The formulation of the regulation policy for a partial-regulated machine is resumed in Tab. 3.3.

	Region II	Region II1/2	Region III
$\lambda_{ref}(V)$	$\arg\max_{\lambda} C_P(\lambda,\beta)$	$\frac{\Omega_{r,t}R}{V}$	$\frac{\Omega_r R}{V}$
$\Omega_{ref}(V)$	$\frac{\lambda}{R}V$	$\Omega_{r,t}$	Ω_r
$\beta_{ref}(V)$	β such that: $C_P\left(\lambda^{II},\beta\right) - p\cdot\max C_P(\lambda,\beta) = 0$	β such that: $C_P\left(\lambda^{II1/2},\beta\right) - p\cdot\max C_P\left(\lambda^{II1/2},\beta\right) = 0$	β such that: $C_P\left(\lambda^{III},\beta\right) - p\cdot C_{P_r}\left(\frac{\lambda^{III}}{\lambda_r}\right)^3 = 0$
$T_{ref}(V)$	$p\cdot\frac{1}{2}\rho A R V^2\frac{\max C_P(\lambda,\beta)}{\lambda^{II}}$	$p\cdot\frac{1}{2}\rho A R V^2\frac{\max C_P\left(\lambda^{II1/2},\beta\right)}{\lambda^{II1/2}}$	$p\cdot\frac{P_r}{\Omega_r}$

Table 3.3: Regulation policy for partial-regulated machine

The regulation policies is computed off-line for different values of p and provided, in the form of look-up tables, to the model controller. The latter computes the regulation policy for any value of the partialization factor p, simply performing a linear interpolation among the already mentioned look-up tables.

Fig. 3.7 shows the regulation policies for different values of the partialization factor p.

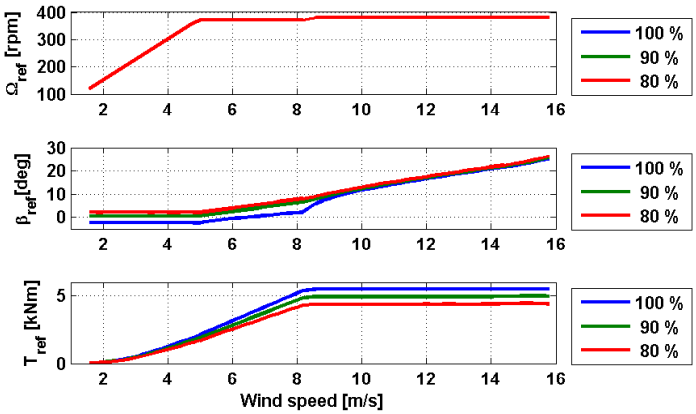

Figure 3.7: Partialized trajectories for rotor speed, pitch and torque

The figure clearly highlights that the partialization of the machine is performed by pitching the blade much toward the incoming wind speed, so as to extract less power.

An analysis was also conduced in order to evaluate the potential of the *ISO-TSR* approach in terms of maximizing the wind farm power production. Indeed, it is clear that partializing the upwind wind turbine means reducing its axial induction factor and therefore reducing the impact of its wake on the power produced by the downstream wind turbine. But, this approach can lead to an increase of the overall wind farm power only if the reduced power produced by the upwind machine is counterbalanced by a substantial increase of the power produced by the downwind machine. It is clear that this last requirement is even more satisfied as greater is the reduction of the axial induction factor once fixed the parzialization factor.

Fig. 3.8 helps to explain how the partialization approach could affect the overall wind farm power. The graph on the left (Fig. 3.8a) shows the rotor averaged axial induction factor A, computed using:

$$A(\lambda, \beta) = \frac{1}{\pi R^2} \int_0^R a(r, \lambda, \beta) r dr \tag{3.14}$$

with $a(r)$ the local induction factor, related to the V2 model, while Fig. 3.8b shows the same data related to a 2MW wind turbine. In both graphs, A is plotted as function of the TSR and of the rotor power coefficients. Moreover, the dashed lines show the variation of A along the regulating set points for different values of the parzialization factor, while the continuous ones mark the constant values of C_P.

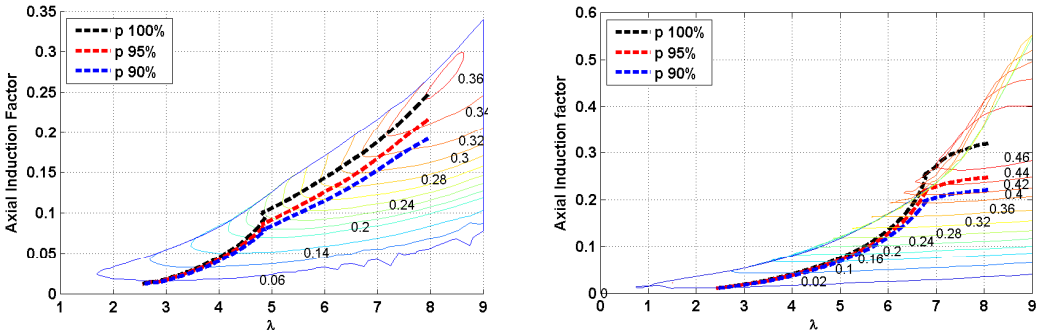

(a) V2 model

(b) 2 MW wind turbine

Figure 3.8: A as funcion of TSR and C_P

If we look at the V2 model data at region II regulating set-point, it is possible to observe that the *ISO-TSR* approach does not seem the best one

in terms of achievable reduction of A once fixed the rotor C_P. Indeed, the axial induction factor can be lower if one makes the wind turbine operate at lower TSR, i.e. lower rotor speed, while it seems not convenient to make the machine operate at higher TSR, i.e. higher rotor speed.

However, it is also possible to observe that the results obtained from the 2MW wind turbine are quite different, since the axial induction factor is almost constant for a wide range of TSR. The reason of this difference is principally imputable to the Reynolds mismatch between the V2 model and the real wind turbine, whose main effect is the reduction of the V2 axial induction factor at maximum C_P.

Given the above considerations, we can say that partialize a full-scale wind turbine using the *ISO-TSR* approach would leads to results similar to those that would be obtained with a different partialization approach, in terms of increase of wind farm power. If we instead look at how partializing the V2 model, we got that making the rotor rotate at lower speed could moderately increase the wind farm power production, but at the cost of an higher complexity in the integration of this control strategy within the model control system. Indeed, adopting the *ISO-TSR* allows to do not change the model control system described in paragraph §3.1.2, given that only changes of torque target and minimum pitch are required.

Furthermore, it is important to remind that changing the TSR when partializing the machine means changing the rotor speed, which could imply important consequences on load spectra and therefore on fatigue. These issues have not been investigated in this research work, but will certainly be in the next future.

3.3 Wind farm control

In the literature, it is possible to find two different approach situable for the wind farm control. In the first case, the wind farm control is provided by one of the wind turbine controllers, i.e. it is integrated in a preexisting control structure. The second approach aims to keep the wind farm control separated from the wind turbine one, so it is possible to store the wind farm control hardware in a more comfortable location, for example, in an on-shore location (for off-shore wind farms), and to manage the wind turbines through remote control. The latter approach gives an important advantage, i.e. it prevents that the breakdown of the wind turbine on which wind farm control runs could compromise the management of the entire wind park, thus increasing the reliability of the wind farm controller.

For these reasons, in the present work, we aimed to realize the wind

farm controller following the second approach, which is also suitable for wind tunnel testing.

As explained in paragraph (§2.2.2), each wind turbine of the wind farm is equipped with a `M1 Bachmann` hard real-time system that provides for each control (see §3.1). The wind farm controller, then, has to be integrated in a new hardware and must communicate with each wind turbine. Moreover, it must provide a graphical interface that allows an operator to manage the experiments (start/stop the wind farm controller, change set points, etc.) and it must allow the possibility to easily extend the wind farm control to more than two wind turbines.

3.3.1 Wind farm control – wind turbine control communication

During the project phase of the wind farm controller, it became clear that the wind farm controller does not need to be run on an hard real-time hardware, because characteristic timescale for wake diffusion and propagation within the wind tunnel is in the order of some seconds. Keeping in mind this consideration, it is evident that the wind farm control can be developed on a less sophisticated hardware, like a Desktop PC. For this reason, the system has been developed on a Desktop PC with a `Windows` operating system.

Different solutions were possible, concerning the communication between a `Windows` pc and the `M1 controller`:

- `M-target for Simulink`: allows the communication between `Windows` and `M1 controller` through the use of `Simulink`. This package represented the most suitable solution, considering the great simplicity in interfacing with `Matlab` codes and that, nowadays, `Simulink` represents a software widely used for industrial applications; nevertheless, this solution was discarded because it results too economically costly for academic applications.

- `OPC client`: a software interface standard that allows Windows programs to communicate with industrial hardware devices and which is implemented in server/client pairs. The OPC server is a software program that converts the hardware communication protocol used by a PLC into the OPC protocol. However, also this solution was discarded because the available Standard OPC server had some limitations concerning number of clients/variables and because the choice of this solution needed a strong background in `OPC client and server` communication, thus requiring long developing time.

- `M1com.dll`: a license-free C/C++ library that can be directly used in windows applications. This solution was chosen for several reasons: there were no limitations in the number of variables, as in `OPC` solution, the programming language is known for its capacity to provide highly efficient codes and fast developing time was possible since C/C++ programming languages is well know by the author.

For the reasons explained in the previous overview, the wind farm controller, here called "*Super-controller*", has been developed as a system external to the `M1 Bachmann`: it consists in a C developed program running on a `Windows` operating system that communicates with the two wind turbine controllers through a simple `Ethernet` connection. Thanks to the `M1COM` library, provided by `Bachmann`, it was possible to have a remote access to both `M1 Bachmann` systems, reading and writing their variables, copying/trasfering files and other operations.

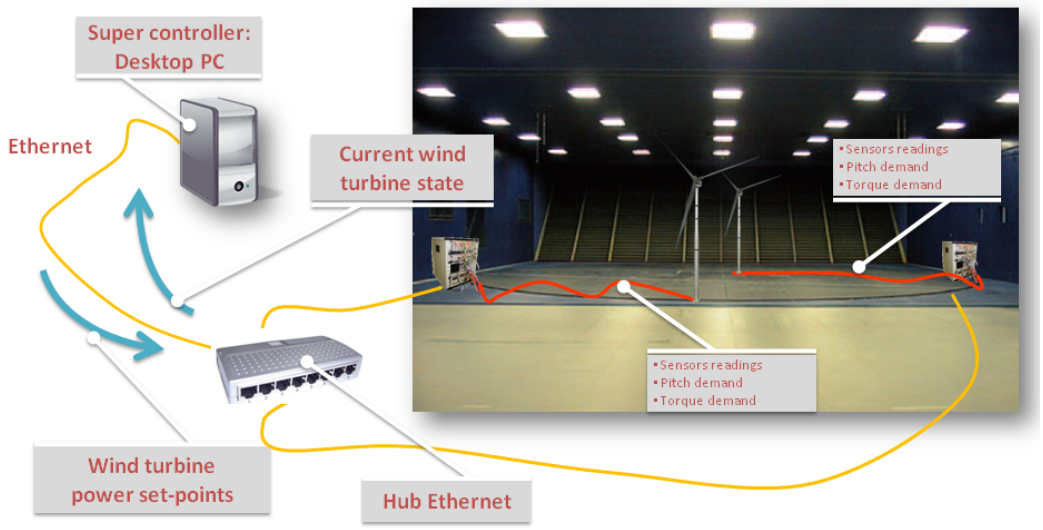

Figure 3.9: Super-controller conceptual scheme

In Fig. 3.9, the wind farm layout is presented. The wind turbines are placed in the wind tunnel and communicate with their respective `M1 controllers`, while the Super-controller is placed outside the wind tunnel, i.e. in the control room, and communicates to controllers thanks to an Ethernet hub.

It is necessary to distinguish two main levels in the wind farm controller: the super-controller level and the wind turbine controller level, because they operate complementary roles in the wind farm control. The super-controller

role is to run an optimization algorithm and to send power set-points, expressed in per cent of full-scale power, to the wind turbine controllers, whose role is adjusting the torque/pitch actuator outputs so as to accomplish to the super-controller requests.

As stated in paragraph §3.2, regulation policies are computed off-line for several user-defined partialization factors and stored inside the hardware memory of the wind turbine controller. The latter receives the power set-point from the super-controller and linearly interpolates among the stored data to get the regulation policy at desired partialization factor. When the super-controller changes the power set-point of a wind turbine the variation of the wind turbine power is not immediate. Indeed, let's define P^n_{s-p} the new power set-point, required by the wind farm control and P^o_{s-p} the previous power set-point. The wind turbine controller will gradually apply the power set-point P^*_{s-p}, defined as:

$$P^*_{s-p} = \begin{cases} P^o_{s-p} + P_{grad}(t-t_0)\,\mathrm{sgn}\left(P^n_{s-p} - P^o_{s-p}\right) & \text{if } t < t_0 + \frac{\left|P^n_{s-p} - P^o_{s-p}\right|}{P_{grad}} \\ P^n_{s-p} & \text{if } t \geq t_0 + \frac{\left|P^n_{s-p} - P^o_{s-p}\right|}{P_{grad}} \end{cases} \tag{3.15}$$

where t_0 is the time when P^n_{s-p} was required, while P_{grad} tells you how fast P^n_{s-p} will be reached. This strategy allows to gradually change the wind turbine power thus avoiding to overload the actuators and reducing transient-related loads.

3.3.2 Super-controller architecture

The super-controller (**SC**) allows the operator to control the wind farm (**WF**) in two different modes, here defined **Automatic** and **Manual**. If neither of the two is activated by the operator, the system automatically switches to the a third one, here named **No Mode**, in which the wind turbines (**WT**s) are individually regulated (as described in §3.1), therefore, no wind farm control is performed. Fig.3.10 shows with a diagram the logic governing the **SC**. The **SC** starts establishing the communication with the `M1` controllers; if something goes wrong in this phase, the system returns an error message. Once completed this preliminar phase, the **SC** enters in an loop and waits for the activation of one of the two modalities; during this period the system remains in **No Mode**.

3.3.2.1 Manual mode

The manual mode has been conceived to test the communication **SC-WTs** in the initial phase of the **SC** development and , when necessary, to manually

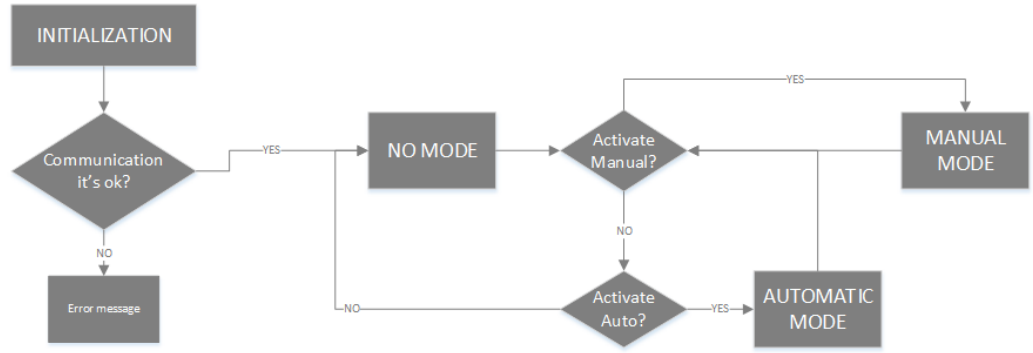

Figure 3.10: Super-controller scheme

regulate the wind turbines power. When the **SC** is set in **Manual**, the users can visualize the current power set-points, define new set-points for each machine, set how much is necessary to wait before starting measuring the **WT** powers and also define the recording time.

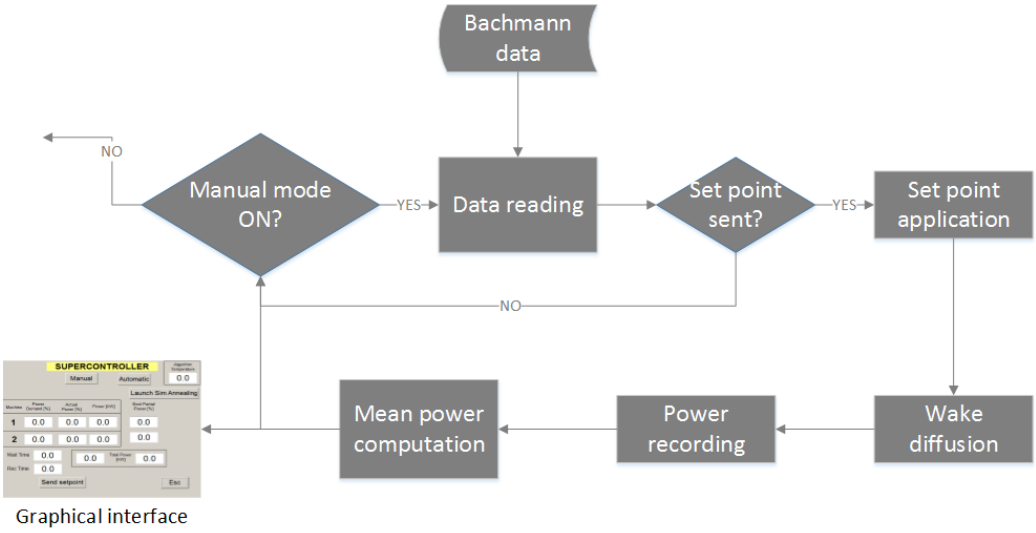

Figure 3.11: Manual mode scheme

If the manual mode is active, the **SC** continuosly reads the **WT**s power until the operator define a new set-point. When this happens, the **SC** communicates to the **M1** controllers the prescribed wind farm regulation and waits until the **WT**s delivery the desired power; the system then waits that the variations of the wake shape and speed deficit propagate throughout the **WF**, records the **WT**s power for a user-defined amount of time and graphically provides to the user the time-average of the recorder data.

3.3.2.2 Automatic mode

The automatic mode represents the core part of the **SC**, because in this modality the system autonomously and real-time regulates the wind farm, following the logic represented in Fig.3.12.

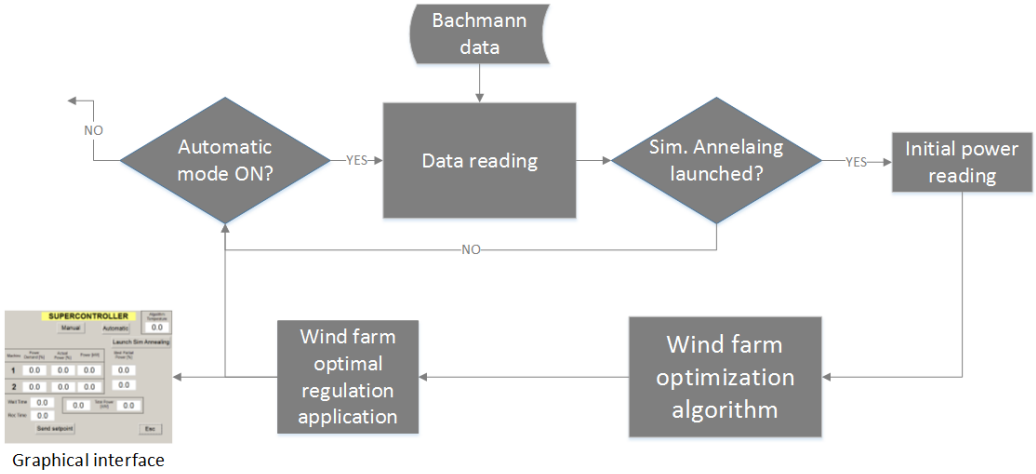

Figure 3.12: Automatic mode scheme

When the **Automatic** mode is selected, the system waits until the operator makes run the algorithm that seeks for the **WT**s power set-points that maximize the wind farm power. At this stage, it is important to clarify that several algorithms could perform effectively this task, and some of those were discussed in the introduction. In the research activity object of this thesis, we have adopted an algorithm based on Simulated Annealing (**SA**) optimization, that will be described in the following paragraph §3.3.3. When the user makes run the **SA**, the **SC** first reads the current **WF** regulation, sets the latter as starting condition and suddenly starts seeking for the best **WF** regulation based on **SA** logic. When the optimization process is completed, the best solution found becomes the wind farm optimal regulation and the system waits for a new user-input. It is important to highlight that this procedure works well within the wind tunnel environment, where the wind speed can be kept constant for the time required by the system to identify the optimal regulation. A different approach should be developed in the future for applying the **SC** logic to the real world.

3.3.3 Simulated Annealing

Simulated annealing is a generic probabilistic metaheuristic algorithm for the global optimization problem. It was proposed by Kirkipatrick, Gelett

and Vecchi (1983) [22] and Cenry (1985) [23] with the aim of finding global minimum of cost functions that may possess several local minima. Despite the lack of a rigorous theoretical justification of its speed of convergence (see [24]), researchers have extensively used **SA** since its introduction, and many papers discuss its applications to a large quantity of well-known problems, like the traveling salesman problem (TSP), the graph partitioning problem (GPP), the graph coloring problem (GCP) and number partitioning problem (NPP) [25–27]. Thanks to its simplicity, **SA** had been applied also to a large number of engineering optimization problems of different nature, and some of these are described in [28].

The name comes from annealing in metallurgy, a technique which involves heating and controlled cooling of a material with the aim of increasing its crystals size while reducing their defects. What the algorithm basically do is randomly exploring the solutions space seeking for the global minimum; this is achieved by comparing a new solution with the saved best one and updating the latter if the new solution is associated to a lower value of the cost function. However, during its exploration process, the **SA** is allowed to accept as best solution also a solution associated to higher value of the cost function; this is one of the most important property of metaheuristic algorithms, since it allows to reduce the risk to find a local optimum instead of the global one. However, the probability of accepting worse solution gradually decreases as the optimum seeking process evolves: this is how cooling is translated in the **SA** algorithm.

3.3.3.1 The algorithm

An **SA** optimization process has been therefore developed to real-time maximize the power produced by the WT^2 wind farm. The implemented algorithm has been represented the scheme in Fig. 3.13:

The here reported scheme allows to understand that the evolution of the **SA** algorithm is driven by the temperature T. This latter decreases following a pre-assigned schedule and its main role is affecting the probability of accepting a non-improving solution. When temperature is still high, the probability of accepting a worse solution is high and the optimizer has the ability of jumping out from local minima. When temperature decreases the chance of acceptance diminishes. The process continues until the temperature becomes lower than a fixed value.

Looking at Fig. 3.13, it is possible to understand that there are some issues to be faced with when adopting the **SA**. It is known that as higher the number of solutions seeked by the **SA** is, as closer to the global optimum the final solution will be. However, it is essential to consider that we want

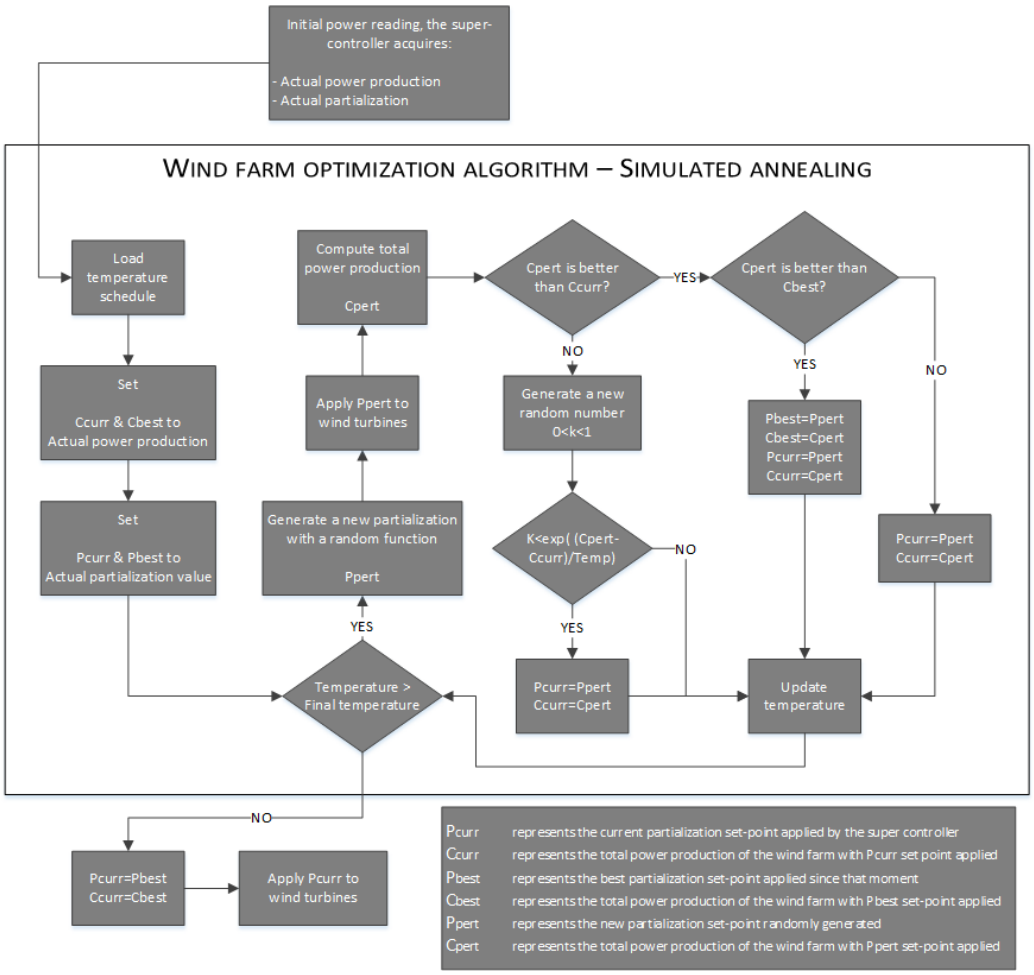

Figure 3.13: Implemented simulated annealing algorithm scheme

to use this algorithm for real-time controlling the wind farm within the wind tunnel, and it is important to take into account for the time required by wakes to propagate. In Tab. 2.1, it is reported that the time for V2 models is accelerated up to almost 23 times, this lead to the fact that time required in a real size condition wake propagation will be about 23 times time required in the wind tunnel, for this reason the controller must be as faster as possible in finding the optimum wind farm operating condition.

Considering this limit, the algorithm has been slightly modified, adding a parameter that records the best solution, allowing a sure convergence with a lower number of iterations. However, it is important to highlight that the best solution is simply recoded and doesn't affect the solution found by the algorithm.

Eventually, temperature schedule must be chosen in a careful way, a too

low temperature can obstacle the ability of accepting a worse solution, on the contrary, a too high temperature can obstacle the convergence to the right solution.

Therefore, considering the overview proposed, a precise calibration of temperature schedule is required, in order to offer a fast and precise solution in the real-time environment. For this reason a large number of simulations were performed studying the interaction of the wind turbines in the wind farm, adopting the *Park wake model* that will be explained in the following paragraph.

3.4 Algorithm calibration

As it was explained in the previous paragraphs the Simulated Annealing algorithm need to be calibrated in order to improve the results quality as much as possible with a low number of iteration.

To perform the calibration of the algorithm and compare the results obtained, it was necessary to study the physical phenomenon, in order to better understand the conditions in which it is possible to observe the best improvement. For this reason, a numerical simulation has been performed using a widespread wake mathematical model that was applied to a wind farm made up of two wind turbine, like the one that will be tested in the wind tunnel.

3.4.1 Wake model

The *Park wake model* is a mathematical model widely used to describe the main behaviour of the wind speed downstream the wind turbine. It describes the behaviour of the wake as a wind speed deficit that change as a function of the distance from the wind turbine that generate it.

Considering a single isolated wind turbine the *Park model* describes wind speed as $V(x, r, a)$, where the parameters x and r are represented in Fig.3.14 and a is the axial induction factor. Particularly:

$$V_i(x, r, a_i) = U_\infty \left(1 - \delta V_i(x, r, a_i)\right) \tag{3.16}$$

where $\delta V_i(x, r, a_i)$ represents the deficit of wind speed induced at the point (x,r) by the upstream wind turbine:

$$\delta V_i(x, r, a_i) \begin{cases} 2a_i \left(\frac{D_i}{D_i + 2kx}^2\right) & r \leq \frac{D_i + 2kx}{2} \\ 0 & r > \frac{D_i + 2kx}{2} \end{cases} \tag{3.17}$$

where k is a roughness coefficient (k=0.075 for farmlands k=0.04 for offshore location).

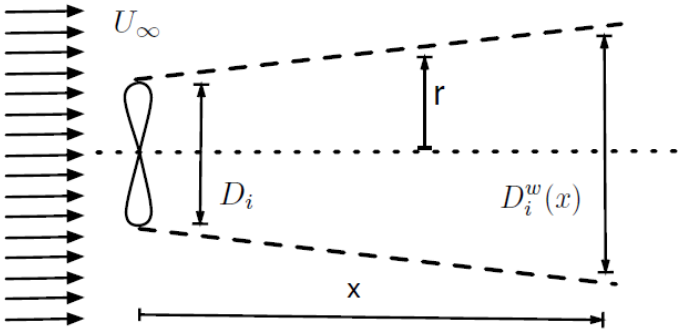

Figure 3.14: Illustration of parameters for Park wake model

The two dominants traits of this model are:

1. The velocity profile is constant along the radial direction of wake

2. The velocity approaches U_∞ at a large distances from the turbine.

Finally, according to Eq 3.17 the diameter of the wake of turbine i at a distance x downstream is given by $D_i^w(x) = D_i + 2kx$.

3.4.2 Wake interaction model

The wake interaction model was described with a common approach present in the existing literature (see Fig. 3.15), in which, rather than deriving an entire velocity profile, an aggregate wind velocity seen by each turbine is used. For any wind turbine, the aggregate velocity is given by

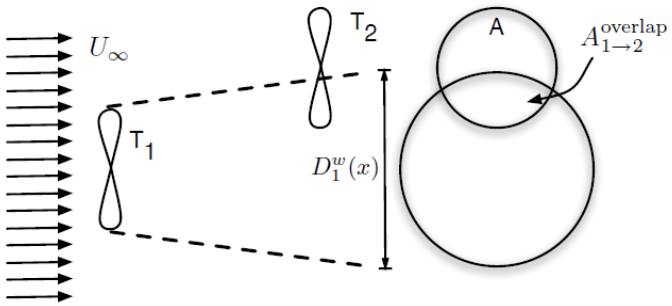

Figure 3.15: Interaction model example

$$V_i(a) = U_\infty \left(1 - \delta V_i(a)\right) \tag{3.18}$$

where the velocity deficit is:

$$\delta V_i(a) = 2\sqrt{\sum_{j \in N: x_j < x_i} \left(a_j \left(\frac{D_j}{D_j + 2k(x_i - x_j)} \right)^2 \frac{A_{j\to i}^{overlap}}{A_i} \right)^2} \tag{3.19}$$

where A_i is the area of the disk generated by the blades of turbine i and $A_{j\to i}^{overlap}$ is the area of the overlap between wake generated by turbine j and the disk generated by the blades of turbine i. According to Eq.(3.18), (3.19) becomes:

$$V_i(a) = U_\infty \left(1 - 2\sqrt{\sum_{j \in N: x_j < x_i} (a_j c_{ji})^2} \right) \tag{3.20}$$

where

$$c_{ji} = \left(\frac{D_j}{D_j + 2k(x_i - x_j)} \right)^2 \frac{A_{j\to i}^{overlap}}{A_i} \tag{3.21}$$

3.4.3 Calibration results

The wind speed values, spreading from the cut-in to the cut-out value have been used to compute the axial induction factor provoked by the upstream wind turbine on the downstream one by means of the `Cp-Lambda` software (see §2.2.4)). For each wind speed the upstream wind turbine partializzation was varied from 80% to 100%, the axial induction factor was computed together with the total power production. The test was repeated changing also the distance between the wind turbines from 2 diameters to 10 diameters and the obtained results are represented in Fig. 3.16.

As we can appreciate from the graph in Fig. 3.16 the power gain increases reducing the distance between the two wind turbines. Moreover, power increase is sufficiently high only with a wind speed lower than 5 m/s, in region II. Therefore, as we can see from the graphs, at 5 m/s the optimum power partializzation moves abruptly from $86 - 88\%$ to $98 - 100\%$.

After having studied the physical phenomenon, the calibration of the algorithm was performed. First of all, let us recall the parameters that play a major role in the algorithm:

- Maximum step (when generating a new perturbation).

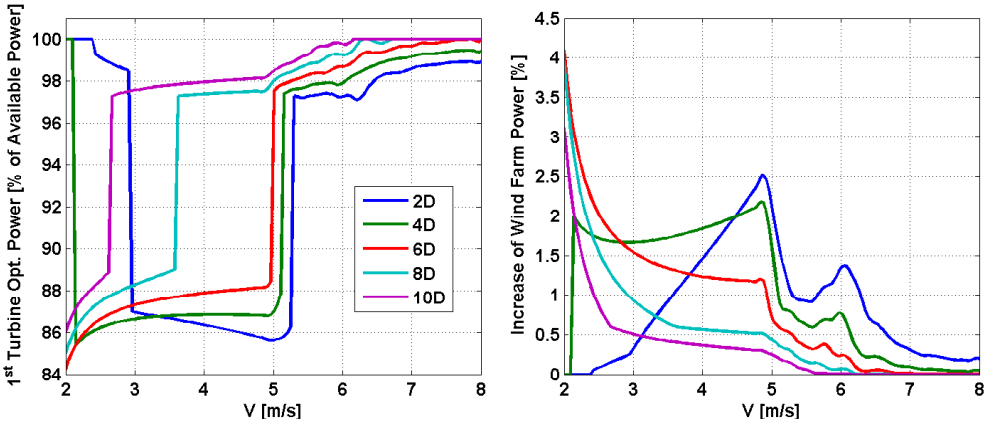

Figure 3.16: Park wake numerical results

- Initial guess.
- Temperature schedule.

The first step was the choice of the strategy for the generation of new partializations. The algorithm generates a new partialization according to Eq. 3.22:

$$p_{pert} = p_{curr} + step \cdot rand(-1, +1) \tag{3.22}$$

where p_{pert} and p_{curr} are respectively the perturbed partialization that the algorithm is going to evaluate and the current partialization applied by the "*Super-controller*" (see Fig. 3.13), *step* is the maximum perturbation that the *Super-controller* can apply, that was fixed to 0.05 in order to allow a sufficient exploration of the solution space and *rand* is a random function that generates a number in the interval $[-1, +1]$.

From Fig.3.16 it can be appreciated that the optimal partialization for all the wind condition considered is in the interval $p \in [0.8, 1]$. For this reason, the initial guess was arbitrarily fixed to 0.9, because during the simulation it was noticed that the solutions presented a certain improvement imposing this initial guess.

Eventually, the most difficult parameter to be set is the third one, i.e. the temperature schedule. Considering the fact that the probability of accepting a non improving solution is given by $\exp(-\frac{\Delta C}{T})$, where ΔC represents the difference between the power measured applying the partialization p_{pert} and p_{curr}, it is evident that the temperature schedule must be changed for every wind speed value,due to the term ΔC, that shows significant variations in every wind speed condition.

The adopted procedure to calibrate the algorithm is the following: the maximum number of iterations was fixed to 50, meaning that in the wind tunnel the test will require $10min$ to be completed, considering a recording time of $10s$ and a waiting time of $2s$ during the experimental test.

After several simulations, it was noticed that the choice of a temperature decreasing with a fixed step wasn't the best solution, since by choosing a too high temperature the algorithm requires too much iteration before starting to reject non improving solutions. By contrast, by choosing a low temperature, the risk was that the behaviour of the algorithm was limited to rejecting non improving solutions. So, it has been considered necessary to define the temperature schedule in a different way as described in Eq. 3.23.

$$[T_1 : z_1 : T_2 + \delta, T_2 : z_2 : 0] \tag{3.23}$$

where z_1 and z_2 are:

$$\begin{cases} z_1 = \frac{T_1 - T_2}{15} \\ \\ z_2 = \frac{T_2 - 0}{35} \end{cases} \tag{3.24}$$

$T1$ and $T2$ have been set and scheduled individually for each wind speed. This kind of approach allows to divide the algorithm in two phases: the first one, in which the probability of accepting non improving solution is higher, but concerns a limited number of iterations; the second one, in which the probability of accepting worse solution is reduced and the number of iteration is increased.

Once the above described parameters have been tuned, the optimization algorithm was tested 100 times in order to verify the convergence to the optimal partialization. The results have been resumed in Tab.3.4.

From Tab. 3.4 it is possible to observe that the algorithm solutions has a mean value close to the optimal one, but its standard deviation is high. The reasons of the dispersion are mainly two. The first one is the fact that the algorithm implements two random functions both to generate new solutions and to accept the non improving one. The second one is the fact that the number of iteration is too low and the convergence not completely reached. However the recorded best solution shows a considerable lower dispersion, this result justify the presence of this parameter and it allows to find a optimal result more close to the expected one.

	Best solution		Algorithm solution	
Wind speed	Mean value	Std.dev.	Mean Value	Std.dev.
$4m/s$	0.8696	0.0016	0.8699	0.0058
$5m/s$	0.8711	0.0015	0.8706	0.0044
$6m/s$	0.9789	0.0018	0.9789	0.0024

Table 3.4: Algorithm calibration results

3.5 Wind farm control testing on test bench

Considering the high costs required to test the wind farm and its controller in the wind tunnel, it is necessary to verify and test the wind farm performance outside the wind tunnel, through a hardware-in-the-loop test.

The main purpose of this test is to obtain experimental results to compare them with the numerical ones presented in the previous paragraphs, and to verify if it is possible to find a match between them despite the inevitable presence of measuring noises.

3.5.1 "*ISO-TSR* approach testing on test bench"

First of all it is necessary to verify if the "ISO-TSR" (described in §3.2.1), approach was implemented correctly and if the wind turbine control was able to follow a partialized trajectory and to switch from a partialization to another without trouble of any nature.

In Fig.3.17 the results of the tests performed setting the wind turbine at different partialization values and changing the wind speed value are represented. This test was performed in order to verify the ability of the wind turbine controller to follow a certain partialized trajectory. In particular, in Fig.3.17a is represented the trajectory at the 60 % of the available power, in Fig.3.17b the trajectory at the 80 % of the available power and in Fig.3.17c the trajectory at the 100% of the available power.

The tests represented in Fig.3.17 have been performed imposing to the wind turbine a wind condition with 10% of turbulence level to verify the strength of the control. In these graphs the trajectories given to the wind turbine controller and the experimental results recorded during the test are

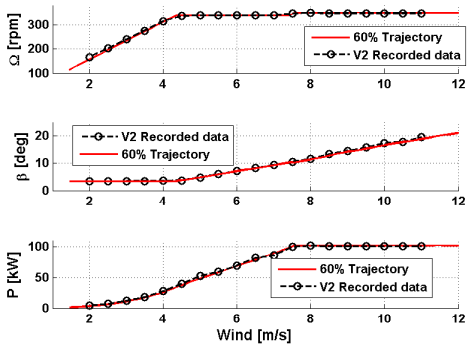

(a) Trajectories at 60 % of the available power

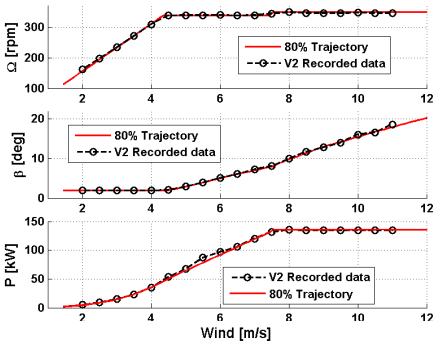

(b) Trajectories at 80 % of the available power

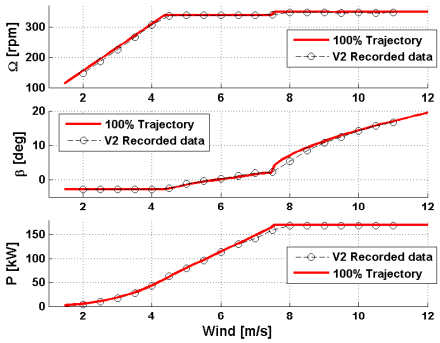

(c) Trajectories at 100 % of the available power

Figure 3.17: Trajectories at 60 %, 80% and 100 % of the available power with 10 % of turbulence realized at test-bench

represented in the same graph. As we can see from the figure, the two curves are substantially overlapped in all the operative range of wind speed, so, it is possible to affirm that the wind turbine controller is able to follow the partialized trajectory in all the three conditions with a limited error.

After having proved that the wind turbine controller is able to follow the assigned trajectory also in a turbulent condition, some transition tests have been performed in the Region II, II1/2 and III, and the results have been resumed in Fig.3.18.

As we can appreciate from the figure, the wind turbine controller is able to change the partialization reference without problem, passing from 100% to 60% and viceversa in in 4 seconds , following the gradient imposed by the wind turbine controller of 10 [%/s], and described in Eq.3.15.

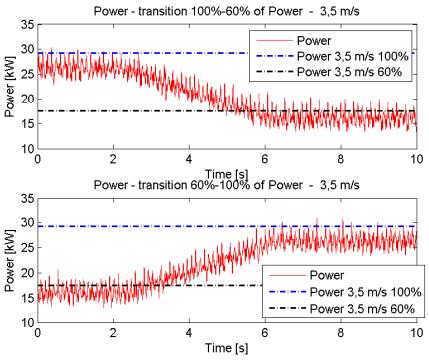

(a) Transions in region II

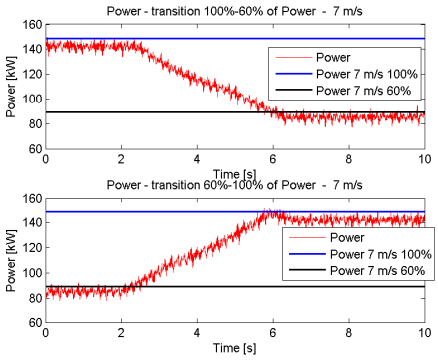

(b) Transions in region II1/2

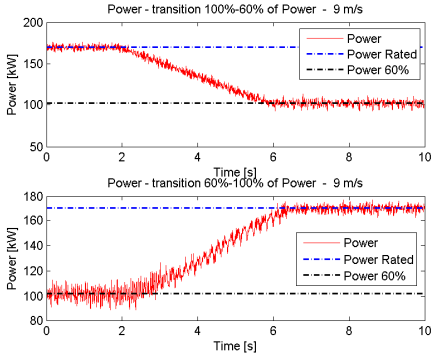

(c) Transions in region III

Figure 3.18: Transition examples at 3.5 m/s, 7 m/s and 9 m/s

3.5.2 Wind farm testing on test bench

Once proved the ability of the wind turbine controller to follow the required trajectory, the next step before the test in the wind tunnel is the test on the test bench.

However, at the present moment, the instrumentation required for the test bench testing (see paragraph §2.2.3) is available only for one of the two wind turbines, for this reason, it is necessary to explain the way this kind of tests have been carried on.

The tests are realized testing the upstream wind turbine on the test bench and applying a known wind speed value. Then, the *Super-controller* records the Torque, the Rotor Speed and the Axial induction factor (see Eq.3.14) of the upstream wind turbine in a time span of 10 seconds. After having recorded these parameters and having saved them in a file, the *Super-controller* computes the mean power value of the upstream wind turbine

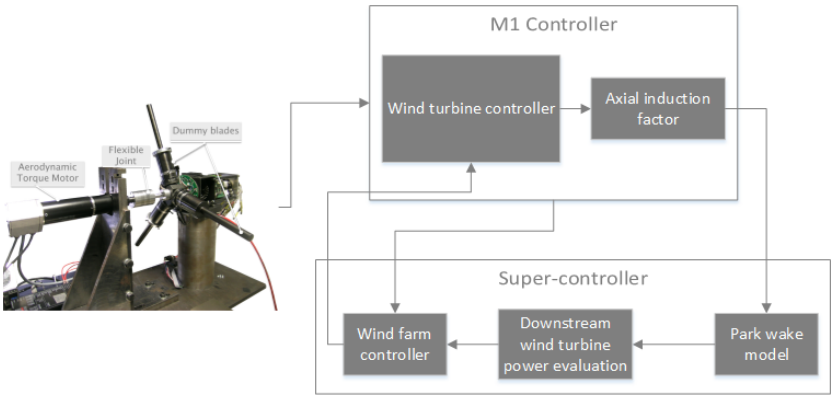

Figure 3.19: Hardware-in-the-loop test scheme

as:

$$P_1 = T \cdot \Omega \tag{3.25}$$

being P the power, T the torque and Ω the rotor speed. After that, the *Super-controller* used the value of Axial induction factor to apply *Park wake model*(see §3.4.1), in order to reproduce the effect of the wake on the downstream wind turbine, obtaining the wind speed operating on it and consequently using this value to compute the mean power production of the downstream wind turbine, as explained in Eq. 3.26.

$$P_2 = P(V(A(\lambda, \beta))) \tag{3.26}$$

Eventually, the total wind farm power production is then obtained as the sum of the two contributes.

$$P_{tot} = P_1 + P_2 \tag{3.27}$$

Before showing the results obtained testing the wind farm on the test bench, it is important to highlight some considerations.

As explained in the previous chapters, the V2 models are subject to a mismatch on the Reynolds number as effect of the scaling procedure. This kind of mismatch leads to important effects on power and on torque, when the wind turbines are tested in the wind tunnel, especially in Region II and II½. In ref. [2] a procedure has been developed in order to compensate this effects, modifying the regulation trajectories.

Nevertheless, the Reynolds effects have never been implemented in the mathematical model of the test bench (on which we are going to test the wind farm) and, for this reason, the wind turbine regulation trajectories have been modified ignoring the compensation methods.

By modifying the wind turbine regulation trajectories, the graphs showed in Fig. 3.16 are no longer valid and, for this reason, they have been computed again and represented in Fig. 3.20.

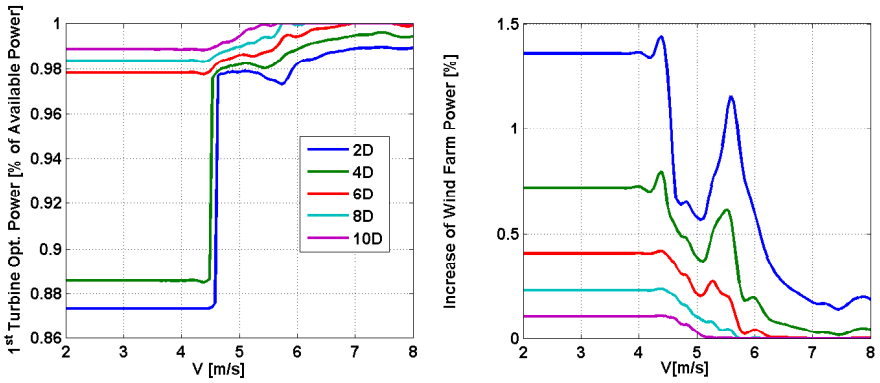

Figure 3.20: Park wake numerical results without including Reynolds effects

By comparing the graphs of Fig.3.20 and Fig.3.16, it is possible to appreciate some differences. First of all, it possible to observe that the behaviour of the optimal partializations is different, especially at low wind speeds, where the optimal partialization remains constant from 2 m/s up to about 4.5 m/s. Secondly, the increase of power in terms of percentage of power is substantially reduced, indeed, positioning the downstream wind turbine at a distance of about 4 diameters, the maximum increase is reduced from about 2.5% to less than 1%.

Despite the low increase of power, the tests have been performed simulating the downstream wind turbine at a distance of 4 diameters at the wind speed condition of 3.5 m/s, 4 m/s, 5 m/s, 6 m/s and 7 m/s. It was considered useless testing the wind farm at higher wind speed conditions, because, as it is possible to see in Fig.3.20, the optimal partialization of the upstream wind turbine is too close to 100% and the power increase is so poor that probably the system would not be able to catch a significant variation of power.

3.5.2.1 Results

In Fig. 3.21a a comparison between the numerical and the experimental results obtained in terms of optimal partialization has been represented.

As we can see, through the experimental tests, it was possible to obtain optimal partialization values similar to the numerical ones. In particular, the better results have been obtained at the wind speed of 3.5 m/s and 6 m/s.

In the other wind speed conditions the discrepancies are higher, but the latter can be considered overall satisfactory because they catch the macro-

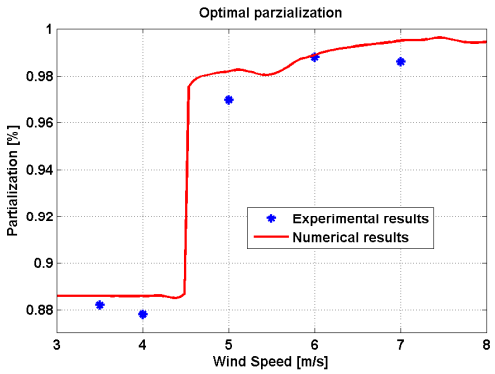

(a) Optimal partializzation vs wind speed: experimental and numerical results

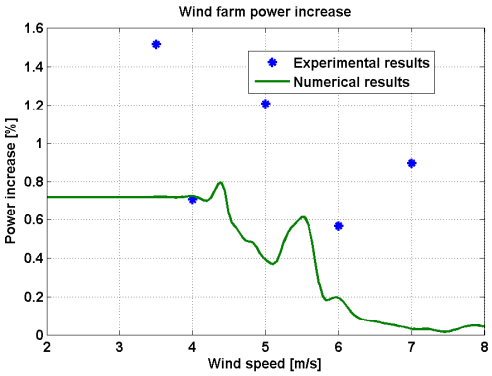

(b) Power percentage increase test bench testing: experimental and numerical results

scopic physical phenomenon, particularly, the "jump" between 4 m/s and 5 m/s.

The wind farm power increase, measured through the experimental tests on test bench is compared to the one computed numerically in Fig. 3.21b, having defined the wind farm power increase as in Eq. 3.28:

$$\Delta P = \frac{P_{tot_{opt}} - P_{tot_{100\%}}}{P_{tot_{100\%}}} \tag{3.28}$$

From this figure it is possible to see that only one of the test performed (the one at 4 m/s) has obtained the expected increase of power, while all the other tests have given an increase of power higher than the expected one.

Nevertheless, it is necessary to consider the fact that the optimal power increase obtained with the numerical simulation was very low, for example, at the wind speed condition of 3.5 m/s, the numerical power increase is 0.72% and considering that the total power production, without partializing the upstream wind turbine, is approximately 38.6 kW, the power increase should be about 0.3 kW instead of 0.6 kW, as measured by the *Super-controller*.

This difference is principally due to a measuring noise that affects the measure of the mean power production of both the two wind turbines. Ideed, looking at Fig. 3.22, in which the wind farm total power production, measured during the tests, for several partialized condition under the wind speed of 3.5 m/s, has been represented together with the numerical results computed in the same conditions, it is possible to observe that two measures performed at similar partialization values can give two total power production values considerably different.

Despite the discrepancies between the values of experimental and numerical power increase, the tests can be considered a success, since, the

"*Super-controller*" was able to catch the optimal partializzation.

However, considering the fact that a so low power increase is given by a limit imposed by the test bench mathematical model, it is clear that in the wind tunnel testing, having the opportunity to test the wind farm with a higher expected power increase (see Fig. 3.16), the measure of the power will be more reliable and the measured power increase probably will be more close to the numerical one.

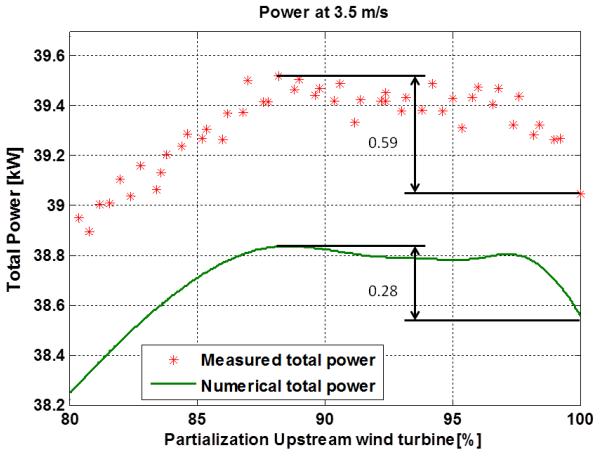

Figure 3.22: Wind farm total power production partializing at wind speed 3.5 m/s

Eventually, having explained the cause of the differences in the power increase values, it is necessary to clarify the nature of the discrepancy that it is possible to appreciate at the wind speed condition of 3.5 m/s between the experimental and the numerical results in terms of total power production(see Fig.3.22). This discrepancy can also be observed in the major part of the tests performed, as it is possible to see from Fig. 3.23, even if, it must be said that the gap is emphasized by the different scale of the graphs.

Having assumed from ref. [2], that the error on torque measure is approximately $E_T = 0.002Nm$ and that the error on rotor speed is $E_\Omega = 2rpm$, in Fig. 3.23, the error associated to the measures and described in Eq. 3.29 has been represented.

$$E_P = T \cdot E_\Omega + \Omega \cdot E_T \tag{3.29}$$

It is possible to affirm that the discrepancy is probably due to an offset error happened during the measures, but, above all, the results can be

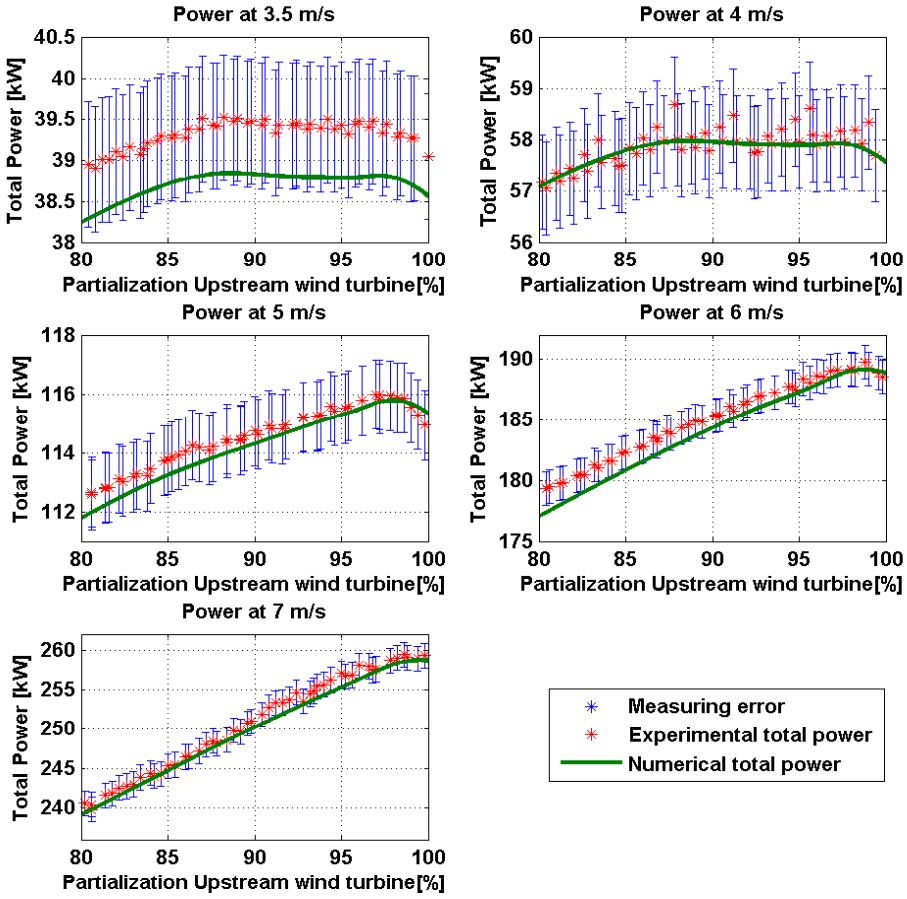

Figure 3.23: Wind farm total power production partializing at the wind speed: 3.5 m/s, 4 m/s, 5 m/s, 6 m/s and 7 m/s. Numerical and experimental results

considered satisfactory, as they allow to reproduce the physical phenomenon with a certain precision.

Chapter 4

Conclusions and future developmets

4.1 Conclusions

The present thesis work has presented the development of a real-time wind farm controller for wind tunnel applications.

The strength of this work is the fact that the developed controller is able to control a wind farm in the wind tunnel. The wind tunnel experimentation represents, at the present moment, a great opportunity for the wind energy research, but particularly for wind farm control research, indeed, in this environment it is possible to study the effects of a real wake generated by the upstream wind turbine on the downstream one and, for this reason, to obtain results more close to the full scale wind turbine, instead of mathematical models that are not able, at the present moment, to describe the complete physical phenomenon. Moreover, the wind tunnel requires more reliable control solution, avoiding the study of such control solution that unattainable on the real wind farms and allowing to face those problem that a theoretical study can't present.

First of all, this work has presented how the wind turbine control has been integrated in the wind farm control thanks to the "*ISO-TSR*" approach, which represents the control policy developed to reduce the power of the upstream wind turbine in order to reduce the effects of its wake on the downstream one. The strength point of this approach is its simplicity and the fact that it allows to improve the wind farm total power without changing the rotor speed of the wind turbine in the same wind speed condition, so reducing the probability to come across changes in the load spectra an so on fatigue phenomena. However, the price to pay is the fact that this solution may be suboptimal, as explained in §3.2.1, but a deeper investigation is required in

the future in this field.

Secondly, after having developed a wind farm control policy, it was described the development of the real-time wind farm control, a C based code, able to provide the communication between a Desktop PC running a Windows operating system and the two `Bachmann` systems that provide the wind turbine control. The implemented system is also able to read and write variable from the `Bachmann` system, so, it is able to send set-points and take some measures.

The developed graphical interface, which allows to an operator to interact with the system, represents a key element, it allows the change of the wind controller parameters in every moment and the real-time monitoring of any variable.

The control architecture and communication of the system has been fully described. The controller allows a manual regulation of the wind turbine, but also an automatic regulation, according to any optimization control law. In this application, the *Super-controller* was equipped with a "*Simulated Annealing*" algorithm. The algorithm optimization choice doesn't have the pretension of being the best solution for wind farm power optimization, indeed, even if the algorithm converge to solution closed to the optimal one in 10 minutes, it must be considered that in wind tunnel time 23 times faster than in full scale application.

This algorithm represents only an application example in order to prove the ability to real-time controlling the wind farm in the wind tunnel. Indeed, the *Super-controller* was conceived in the perspective of being versatile, so the optimization algorithm can be rapidly changed, flanked or integrated with other optimization algorithms that have to be tested in the wind tunnel.

The wind farm control has been successfully tested on the test bench, showing the ability of the wind turbine controller to follow an assigned partialized trajectory and to switch from a partialization to another following an assigned gradient. It was proved also the ability of the optimization algorithm to find the optimum value of power production.

The expected and the measured results that have been reported in this work are different from the ones that we will see in the wind tunnel, because of the reasons explained in §3.5.2. However, considering the ability of the *Super-controller* to measure the power increase and considering the higher power increase expected in the wind tunnel, the wind tunnel experimentation will show results even better than the ones obtained on the test bench.

Eventually, it is necessary to remark the fact that the tests in the wind tunnel couldn't be performed because of the failure of the torque measuring set-up on one of the two models. This failure has made impossible the test in the wind tunnel, which will be scheduled once the failure will be fixed.

4.2 Wind tunnel testing

First of all, it is necessary to highlight that it wasn't possible to perform the tests in the wind tunnel in good time to be presented in this thesis work, because of the failure that happened to the conditioning card of the strain gauges to one of the two V2 model before the tests. The failure has made impossible the torque measure and so the control of one of the two wind turbine, for this reason, it was impossible for us to perform any kind of test with this model, the wind tunnel tests have been postponed and they will be scheduled again once the model will be repaired.

Therefore, in the following, it will be explained the way the tests will be performed once the failure will be repaired.

4.2.1 Test procedure

The wind-tunnel tests will been carried out placing the second model perfectly aligned with the first one and 4D downstream, as shown in Fig.4.1.

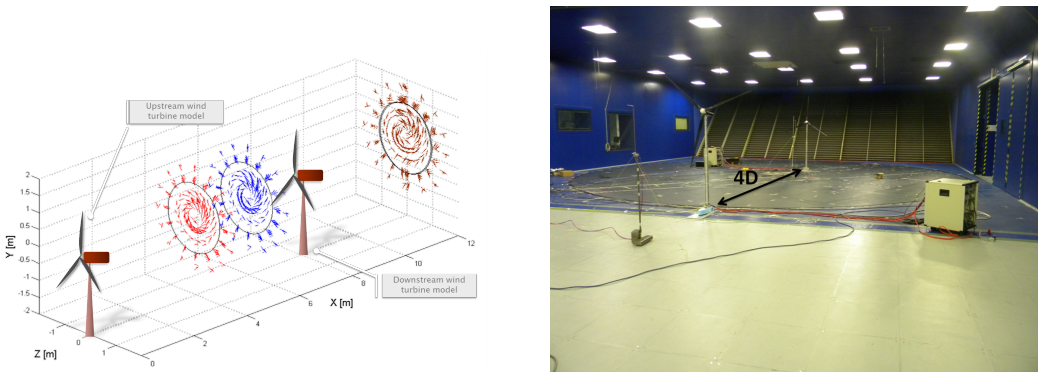

Figure 4.1: Wind tunnel layout for wind farm testing

This configuration will allow to reproduce the wind farm condition test on the test bench, with two important differences: we will have a real power measure of the downstream wind turbine and, above all, the most important feature will be the possibility of having a real wake and not a wind deficit computed by a simplified mathematical as we were forced to do during the test bench tests.

Even if the *Park wake model* allows to reproduce a macroscopic physical phenomenon, the effects provoked by a real wake can't be simply resumed in a simple wind deficit. Indeed, the wake is characterized by a certain turbulence and by a swirl effect on the wind speed which is a function of the rotor speed rotation of the upstream wind turbine.

In this overview, the downstream wind turbine will be interested by a wind speed which is far from being stationary and constant on the rotor speed area. For this reasons, a local wind speed measure, like the one provided by a Pitot tube and a hot wire anemometer will not be apt. It will be necessary to provide a more global information of the wind speed interesting the wind turbine rotor, for example like a wind observer.

The wind farm will be placed in the wind tunnel, while the super controller will be placed outside in command room (see also Fig.3.9), connected to the `M1com` through an Ethernet hub.

As already explained, since the *Super-controller* is not active, the two wind turbines regulate themselves individually, following the control policy explained in §3.1.

After having started the wind turbine controllers, having imposed a certain wind speed value in the wind tunnel, the wind farm controller will be activate, launching the optimization algorithm, that will start to try some partialization until a convergence is reached.

During the test, the *Super-controller* will perform the power measures according to Eq. 4.1

$$P_{tot} = T_1 \cdot \Omega_1 + T_2 \cdot \Omega_2 \tag{4.1}$$

It will save in a file all the required informations, in order to being able during the post processing phase to rebuild the behaviour of the algorithm and the one of the wind farm.

The wind tunnel tests will be performed at different wind speed: 4 m/s, 5 m/s, 6 m/s and 7m/s, i.e the wind speed in which a higher power increase has been foreseen from the numerical results represented in Fig.3.16.

However, it is clear that, since the wind farm is placed in the wind tunnel, the downstream wind turbine will be subject to a real wake and not to a value computed by a mathematical model, so, we expect that the results that we will obtain will be different from the numerical ones. But, having demonstrated the ability of the algorithm to converge to an optimal value and having demonstrated the ability of the *Super-controller* to realize a real-time control we are quite sure that the *Super-controller* will converge to the optimal value whichever it is.

During the tests the loads experienced by the blades and by the tower will also be recorded, and they will be compared to ones recorded during the previous tests, in which the wind farm controller wasn't still realized. This comparison will allow to understand how the ISO-TSR approach interacts with the wind turbines in terms of loads and fatigue.

After having examined the loads experienced by the two wind turbines, a study to develop a wind farm algorithm able to diminish them will be

started.

4.3 Future developments

The developed controller doesn't represent arrival point of the project, but it is only the first step for the future studies on the wind farm control laws.

In the future a wind farm made up of 9 smaller wind turbines for wind tunnel applications will be realized, the "*Super-controller*" developed in this thesis work will represent only the starting point, through which it has been demonstrated that the wind farm control in the wind tunnel is possible.

But, the future studies will not focus their attentions only on the number of wind turbines that the controller will have to manage, indeed, the versatility of this project will allow also to test new control laws.

The Simulated Annealing algorithm, developed in the "*Super-controller*", represents only an example of the possible application. Indeed, thanks to the versatility of this controller, the optimization algorithm can be rapidly changed, for example, with a genetic algorithm or with an algorithm based on the gradient method, or for example an *Simulated Annealing*-Gradient method combined, in which the first one is used to explore, numerically, the solution space and give in few seconds to the second one an initial guess close to optimal solution. This combined algorithm will allow to control the wind farm in a faster way, once found a solution next to the optimal one the gradient method will surely converge to the optimal solution in few iterations.

The present work has focused the attention only on the optimization of the total power production, future developments will surely include also the reduction of the loads operating on the tower and on the blades with a particular attention to the fatigue.

Moreover, one of the limit of this work was the fact that the V2 models were not equipped with yaw actuators, so the power optimization was performed only with pitch actuators. The future studies will includes also the possibility to optimize the problem operating on yaw actuators, which, deflecting the wake direction will allow to improve even more the results obtained in this work.

Bibliography

[1] Paul Fleming, Pieter Gebraad, Jan-Willem van Wingerden, Sang Lee, Matt Churchfield, Andrew Scholbrock, John Michalakes, Kathryn Johnson, and Pat Moriarty. The sowfa super-controller: A high-fidelity tool for evaluating wind plant control approaches. Technical report, National Renewable Energy Laboratory (NREL), Golden, CO., 2013.

[2] Campagnolo F. *Wind tunnel testing of scaled wind turbine models: aerodynamics and beyond*. PhD thesis, Politecnico di Milano, 2012.

[3] Andrew Kusiak and Zhe Song. Design of wind farm layout for maximum wind energy capture. *Renewable Energy*, 35(3):685–694, 2010.

[4] Alireza Emami and Pirooz Noghreh. New approach on optimization in placement of wind turbines within wind farm by genetic algorithms. *Renewable Energy*, 35(7):1559–1564, 2010.

[5] Eduard Muljadi and Charles P Butterfield. Pitch-controlled variable-speed wind turbine generation. *Industry Applications, IEEE Transactions on*, 37(1):240–246, 2001.

[6] Boubekeur Boukhezzar, L Lupu, Houria Siguerdidjane, and M Hand. Multivariable control strategy for variable speed, variable pitch wind turbines. *Renewable Energy*, 32(8):1273–1287, 2007.

[7] Andrew Miller, Edward Muljadi, and Donald S Zinger. A variable speed wind turbine power control. *Energy Conversion, IEEE Transactions on*, 12(2):181–186, 1997.

[8] CL Bottasso, A Croce, Y Nam, and CED Riboldi. Power curve tracking in the presence of a tip speed constraint. *Renewable Energy*, 40(1):1–12, 2012.

[9] Anca D Hansen, Poul Sørensen, Florin Iov, and Frede Blaabjerg. Centralised power control of wind farm with doubly fed induction generators. *Renewable Energy*, 31(7):935–951, 2006.

[10] JW Wagenaar, LAH Machielse, and JG Schepers. Controlling wind in ecn's scaled wind farm. *Proc. Europe Premier Wind Energy Event*, pages 685–694, 2012.

[11] F van Dam, P Gebraad, and Jan-Willem van Wingerden. A maximum power point tracking approach for wind farm control. *Proceedings of The Science of Making Torque from Wind*, 2012.

[12] Kathryn E Johnson and Naveen Thomas. Wind farm control: Addressing the aerodynamic interaction among wind turbines. In *American Control Conference, 2009. ACC'09.*, pages 2104–2109. IEEE, 2009.

[13] Jaejoon Lee, Eunkuk Son, Byungho Hwang, and Soogab Lee. Blade pitch angle control for aerodynamic performance optimization of a wind farm. *Renewable Energy*, 2012.

[14] Maryam Soleimanzadeh and Rafael Wisniewski. Controller design for a wind farm, considering both power and load aspects. *Mechatronics*, 21(4):720–727, 2011.

[15] Jason R Marden, S Ruben, and L Pao. A model-free approach to wind farm control using game theoretic methods. *IEEE Transactions on Control Systems Technology*, 2013.

[16] Maryam Soleimanzadeh, Rafael Wisniewski, and Stoyan Kanev. An optimization framework for load and power distribution in wind farms. *Journal of Wind Engineering and Industrial Aerodynamics*, 107:256–262, 2012.

[17] Thomas Sørensen, Morten Lybech Thøgersen, Per Nielsen, and Niels Jernesvej. Adapting and calibration of existing wake models to meet the conditions inside offshore wind farms. *EMD International A/S. Aalborg*, 2008.

[18] Poul Sørensen, Anca D Hansen, and Pedro André Carvalho Rosas. Wind models for simulation of power fluctuations from wind farms. *Journal of Wind Engineering and Industrial Aerodynamics*, 90(12):1381–1402, 2002.

[19] Anonymous. The wind tunnel of politecnico di milano.

[20] *Cp-Lambda user manual.*

[21] *WIND ENERGY EXPLAINED Theory, Design and Application.* John Wiley & Sons Ltd, 2009.

[22] Scott Kirkpatrick, D. Gelatt Jr., and Mario P Vecchi. Optimization by simmulated annealing. *science*, 220(4598):671–680, 1983.

[23] VLADIMÍR Černỳ. Thermodynamical approach to the traveling salesman problem: An efficient simulation algorithm. *Journal of optimization theory and applications*, 45(1):41–51, 1985.

[24] Dimitris Bertsimas and John Tsitsiklis. Simulated annealing. *Statistical Science*, pages 10–15, 1993.

[25] David S Johnson, Cecilia R Aragon, Lyle A McGeoch, and Catherine Schevon. Optimization by simulated annealing: An experimental evaluation; part i, graph partitioning. *Operations research*, 37(6):865–892, 1989.

[26] David S Johnson, Cecilia R Aragon, Lyle A McGeoch, and Catherine Schevon. Optimization by simulated annealing: an experimental evaluation; part ii, graph coloring and number partitioning. *Operations research*, 39(3):378–406, 1991.

[27] David S Johnson, Cecilia R Aragon, Lyle A McGeoch, and Catherine Schevon. Optimization by simulated annealing: an experimental evaluation; part iii, the traveling salesman problem. *Unpublished manuscript*.

[28] Nazmiye Acikgoz and Carlo L Bottasso. Metric-driven mesh optimization using a local simulated annealing algorithm. *International journal for numerical methods in engineering*, 71(2):201–223, 2007.

[29] *Matlab user manual*.

[30] *Solution center user manual*.